HHS Public Access

Author manuscript

Mol Cell. Author manuscript; available in PMC 2024 September 07.

Published in final edited form as:

Mol Cell. 2023 September 07; 83(17): 3108–3122.e13. doi:10.1016/j.molcel.2023.07.028.

A Zpr1 co-chaperone mediates folding of eukaryotic translation elongation factor 1A via a GTPase cycle

Alexander J. McQuown[1,3], **Anjali R. Nelliat**[1,3], **Dvir Reif**[1,3], **Ibrahim M. Sabbarini**[1], **Britnie Santiago Membreno**[2], **Colin Chih-Chien Wu**[2], **Vladimir Denic**[1,4,*]

[1]Department of Molecular and Cellular Biology, Harvard University, Cambridge, MA 02138, USA

[2]RNA Biology Laboratory, Center for Cancer Research, National Cancer Institute, National Institutes of Health, Frederick, MD 21702, USA

Summary

General protein folding is mediated by chaperones that utilize ATP hydrolysis to regulate client binding and release. Zinc finger protein 1 (Zpr1) is an essential ATP-independent chaperone dedicated to the biogenesis of eukaryotic translation elongation factor 1A (eEF1A), a highly abundant GTP-binding protein. How Zpr1-mediated folding is regulated to ensure rapid Zpr1 recycling remains an unanswered question. Here we use yeast genetics and microscopy analysis, biochemical reconstitution, and structural modeling to reveal that folding of eEF1A by Zpr1 requires GTP hydrolysis. Furthermore, we identify the highly conserved Altered inheritance of mitochondria 29 (Aim29) protein as a Zpr1 co-chaperone that recognizes eEF1A in the GTP-bound, pre-hydrolysis conformation. This interaction dampens Zpr1•eEF1A GTPase activity and facilitates client exit from the folding cycle. Our work reveals that a bespoke ATP-independent chaperone system has mechanistic similarity to ATPase chaperones but unexpectedly relies on client GTP hydrolysis to regulate the chaperone-client interaction.

Graphical Abstract

*Correspondence: vdenic@mcb.harvard.edu.

[3]These authors contributed equally

[4]Lead contact

Author contributions

Conceptualization, A.J.M., A.R.N., D.R., and V.D.; methodology, A.J.M., A.R.N., D.R., I.M.S., B.S.M., C.C.-C.W., and V.D.; formal analysis, A.J.M., A.R.N., and D.R.; investigation, A.J.M., A.R.N., D.R., I.M.S., B.S.M., C.C.-C.W., and V.D.; resources, V.D.; writing – original draft, A.J.M., A.R.N., D.R., and V.D.; writing – reviewing and editing, all authors; supervision, C.C.-C.W. and V.D.; funding acquisition, A.J.M., I.M.S., and V.D.

Declaration of interests

The authors declare no competing interests.

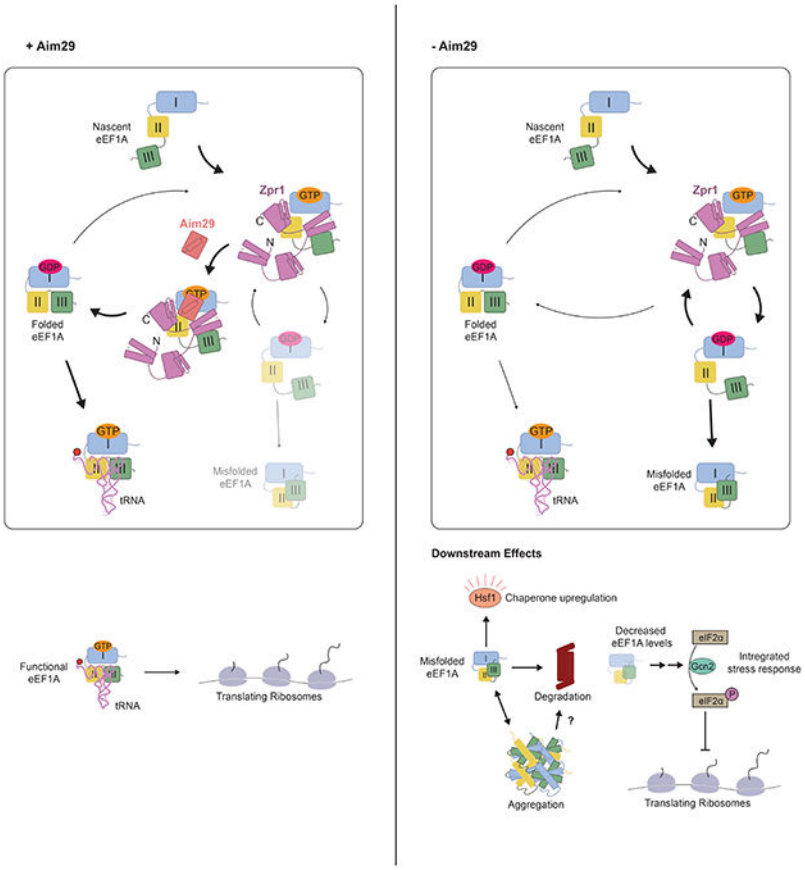

eTOC blurb:

McQuown et al. report that eEF1A folding by its ATP-independent and bespoke chaperone Zpr1 requires client GTP hydrolysis. Furthermore, they uncover the function of the conserved Aim29 protein family as Zpr1 co-chaperones that modulate the eEF1A GTPase folding cycle to facilitate client release and Zpr1 recycling.

Introduction

Folding of newly-synthesized proteins is mediated by molecular chaperones[1]. In addition to their essential housekeeping function, chaperones are effectors of transcriptional responses that counteract protein misfolding and accumulation of protein aggregates following a variety of stress conditions. In budding yeast and metazoan cells, increased activity of the conserved Heat shock factor 1 (Hsf1) results in up-regulation of cytosolic Hsp70 and Hsp90 chaperone systems that collaboratively fold a broad protein clientele[2]. At the core of each system is an ATPase mechanism that regulates cycles of client binding and release[3,4]. Equally critical are co-chaperones that superimpose diverse mechanisms for coupling chaperone-client interactions onto conformational changes driven by ATP hydrolysis[3,4].

Zinc-finger protein 1 (Zpr1) was previously implicated in proteostasis based on its high ranking within Hsf1's stress-induced regulon in the budding yeast *S. cerevisiae*, alongside

components of Hsp70 and Hsp90 systems[2,5]. We obtained functional insight into this prediction by showing that Zpr1's essential function is to fold newly-synthesized eEF1A[6]. eEF1A is a highly abundant and structurally dynamic eukaryotic translation elongation factor. During cycles of GTP hydrolysis, the eEF1A switch regions mediate dramatic movement of their GTP-binding domain (DI) relative to domains II and III (DII and DIII)[7,8]. Our mechanistic dissection of Zpr1 was guided by a ColabFold[9] model of its interaction with an eEF1A folding intermediate that was validated by site-directed mutagenesis studies. According to this view, Zpr1 makes extensive contacts with all three eEF1A domains en route to their stable tertiary conformation. Zpr1's contact with a DI-DII interface is mediated by an alpha helical hairpin (aHH); in addition, Zpr1 uses a zinc-finger (ZnF) to make a hydrophobic bridge between DI and DIII, the latter of which is highly aggregation-prone outside of its normal folding context[6]. The current working model for Zpr1 raises an important mechanistic question: How is Zpr1's interaction with eEF1A regulated to ensure efficient recycling of this ATP-independent chaperone?

ATP-independent chaperones rely on diverse strategies to regulate substrate binding and release in the absence of energy input from nucleotide hydrolysis. Small heat shock protein (sHsp) regulation is achieved by stress-induced disassembly of chaperone-inactive, oligomeric species followed by sHsp co-assembly with misfolded proteins into aggregates poised for substrate reactivation[10]. Other classes of ATP-independent chaperones are tuned to interact weakly with their clients throughout the folding process. This mechanism is best understood for the *E. coli* chaperone Spy, which normally forms low affinity interactions with folding intermediates *and* the native state[11,12]. The ATP-independent chaperone Ric-8 faces a similar challenge to Zpr1 in the context of trimeric G protein biogenesis. In this instance, GTP binding to the G_{α} subunit clients bound to Ric-8 enables them to undergo a conformational change that reduces their affinity for Ric8[13–16]. We have shown using purified components that Zpr1 also requires GTP to structurally stabilize eEF1A, but found no evidence of a folding cycle under these minimal *in vitro* conditions[6]. This suggests flux of newly-synthesized eEF1A through Zpr1 in cells and efficient release of folded eEF1A from Zpr1 under cell-free conditions is mediated by additional factors.

Here we identify Altered Inheritance of Mitochondria 29 (Aim29) proteins, which are broadly conserved in eukaryotes, as Zpr1 co-chaperones. Furthermore, we show that eEF1A GTP binding and hydrolysis enable additional mechanistic steps required for eEF1A folding. Structure-function analysis supports a model in which Aim29 interacts dynamically with a pre-hydrolysis conformational state of the Zpr1•eEF1A folding complex to dampen its GTPase activity and facilitate eEF1A release concomitant with Zpr1 recycling. By comparison to other nucleotide-driven mechanisms of protein folding, our work reveals a surprising similarity between the terminal steps of eEF1A biogenesis and the conformational dynamics of ATPase chaperone systems.

Results

Slow growth of aim29Δ cells is the product of the integrated stress response in counterbalance with an adaptive heat shock response

We previously found suggestive evidence that Zpr1 functions as part of a chaperone system dedicated to folding of newly-synthesized eEF1A[6]. While searching for any such additional components, we noted in TheCellMap[17] the Genetic Interaction (GI) profile similarity between the *zpr1-1* temperature sensitive allele and *aim29*Δ, a deletion of the *S. cerevisiae* gene encoding an uncharacterized but conserved protein[18]. GI profile similarity is a quantitative predictor of gene function, thus suggesting Aim29 is an eEF1A biogenesis factor. To look for additional evidence supporting this prediction of functional similarity, we turned to transcriptional profiling via mRNA sequencing to compare the phenotypes of *aim29*Δ and Zpr1-depleted cells. In the latter, we have previously shown eEF1A misfolding drives induction of Hsf1[6] (Figure 1A), which transcriptionally upregulates cytosolic chaperone systems in response to protein misfolding and aggregation[19,20]. We found evidence of similar protein misfolding stress in *aim29*Δ cells by differential gene expression (DGE) analysis (Figure 1B–C), as well as by using a fluorescent transcriptional reporter of Hsf1 activity (Figure 1D). To determine if Hsf1 staves off proteotoxicity in *aim29*Δ cells, we measured the growth effect of truncating Hsf1's C-terminal activation domain (ΔCTA), which abolishes Hsf1's ability to upregulate gene targets following heat shock but is not required for its essential function in yeast[21–23]. Indeed, the combination of *HSF1ΔCTA* and *aim29*Δ mutant alleles resulted in a severe synthetic growth defect (Figure S1A).

Zpr1-depletion also causes activation of the Gcn4 regulon due to eEF1A depletion (rather than misfolding[6]) (Figure 1A) and we found a similar DGE signature in *aim29*Δ cells (Figure 1B–C). The Gcn4 regulon is the downstream target of a multi-faceted integrated stress response (ISR) that dampens global translation initiation via Gcn2-mediated phosphorylation of eIF2α[24]. At the same time, this mechanism selectively derepresses *GCN4* mRNA translation to enable Gcn4 production, leading to transcriptional up-regulation of numerous target genes, many of which counteract amino acid limitation in the cell[24]. We found evidence of both of these signs of ISR activation in *aim29*Δ cells, which phenocopies Zpr1-depleted cells[6]. First, immunoblotting analysis revealed elevated levels of phospho-eIF2α in *aim29*Δ cell extracts dependent on Gcn2 (Figure S1B). Second, ribo-seq analysis showed *GCN4* mRNA translation was de-repressed in *aim29*Δ cells (Figure S1C), which we confirmed using a fluorescent reporter (Figure 1E). As part of our ribo-seq analysis of *aim29*Δ cells we noted elevated levels of ribosomes with 21 nucleotide (nt) footprints indicative of open A sites[25], suggesting a global defect in eEF1A-mediated delivery of aminoacylated-tRNAs during the elongation cycle (Figure S1D). Lastly, we found the slow growth phenotype of *aim29*Δ cells is suppressed by *gcn2*Δ (Figure S1E), suggesting Gcn2-mediated inhibition of protein synthesis limits their growth. In summary, *aim29*Δ cells share numerous phenotypes with Zpr1-depleted cells suggesting they similarly arise from a defect in eEF1A biogenesis.

The genetic relationship between Aim29 and Zpr1 is conserved in eukaryotes

In addition to their GI profile similarity, TheCellMap also reports the double mutant *aim29*Δ *zpr1-1* results in an aggravating fitness defect[17]. *aim29*Δ cells have normal Zpr1 abundance (Figure S1G) but we hypothesized that Zpr1's specific activity is reduced in the absence of Aim29 to account for the synthetic sick phenotype of the *aim29*Δ *zpr1-1* double mutant. Consistent with this idea, overexpression of Zpr1 from its genomic locus using the strong *TDH3* promoter (*PrTDH3*) restored *aim29*Δ cell growth back to wild-type (Figure S1F and S1H). Critically, *aim29*Δ *PrTDH3-ZPR1* cells no longer show any signs of transcriptional stress characteristic of *aim29*Δ and Zpr1-depleted cells (Figures 1C–E and S1I).

Next, we explored if Aim29's co-functionality with Zpr1 is broadly conserved in eukaryotes. The *S. pombe* Aim29 homolog is encoded by the essential and uncharacterized gene SPAC2C4.04c, and we used two screening approaches to find *aim29*Δ bypass of essentiality (BOE) suppressors. Within a plasmid-based *S. pombe* cDNA overexpression library, we found only plasmids expressing SPAC2C4.04c (*S. pombe AIM29*) or SPAC15A10.04c (*S. pombe ZPR1*) conferred robust growth to *S. pombe aim29*Δ cells (Figure S1J). In the second approach using UV mutagenesis, we identified two independent BOE suppressors mapping to the same amino acid substitution (T353I) at a conserved residue within the *ZPR1* coding region (Figure S1K). We used allelic replacement by plasmid shuffling to introduce the corresponding *S. cerevisiae* Zpr1 (T389I) mutant into budding yeast cells. Zpr1^{T389I} partially reduced Hsf1 activity in *zpr1*Δ*aim29*Δ cells (Figure S1L). Thus, loss of Aim29 homolog function in two yeast species that diverged >100 MYA can be bypassed either by Zpr1 overexpression or a Zpr1 hypermorph.

We also analyzed complementation of yeast *aim29*Δ phenotypes by heterologous expression of C2orf76, the human homolog of Aim29. Overexpressing C2orf76 from a high-copy plasmid partially suppressed Hsf1 induction in *S. cerevisiae aim29*Δ cells (Figure S1M) without affecting the ISR (Figure S1N). More compellingly, strong expression of plasmid-borne C2orf76 from the *nmt1* promoter in *S. pombe aim29*Δ cells resulted in a robust BOE suppressor phenotype (Figure S1O). These findings imply that the mechanism behind Aim29's genetic relationship with Zpr1 in yeast has remained conserved in humans.

Aim29 is an eEF1A biogenesis factor

To look for direct evidence of disrupted eEF1A biogenesis in *aim29*Δ cells, we endogenously expressed Tef1-GFP (eEF1A in *S. cerevisiae* is expressed from two identical coding sequences of *TEF1* and *TEF2* genes) and mCherry-Hsp42, a small Hsp that marks eEF1A aggregates (Tef1-GFP punctae) in Zpr1-depleted cells[6]. Indeed, confocal microscopy revealed a penetrant eEF1A misfolding phenotype that was suppressed by Zpr1 overexpression (Figure 2A).

Next, we measured levels of functional eEF1A in *aim29*Δ cells by taking advantage of Lgt3, a *Legionella* toxin that inhibits eukaryotic eEF1A with exquisite specificity. This enzyme preferentially glucosylates Ser53 of eEF1A that is in a ternary complex with GTP and aminoacylated tRNA[26,27]. In our version of this assay, native cell extracts are incubated with Lgt3 and ^{14}C-labeled UDP-glucose followed by SDS-PAGE; the efficiency of ternary

complex formation is the ratio of ^{14}C-glucosylated eEF1A signal (by autoradiography) and the total eEF1A signal (by immunoblotting). Loss of Aim29 caused a decrease in eEF1A abundance relative to a house-keeping control protein (Pgk1) (Figure 2B), which phenocopies Zpr1-depleted cells[6]. Even more pronounced was the reduction in ternary complex efficiency in *aim29*Δ cells (Figure 2B), which was fully suppressed by Zpr1 overexpression. Mild-overexpression of Aim29 from a low-copy plasmid (*pAIM29*) resulted in a more functional eEF1A population than the wild-type control with empty vector (Figure 2B). *pAIM29* also conferred this effect on wild-type and *PrTDH3-ZPR1* cells (Figure 2B).

Lastly, we measured the biochemical activity of Aim29 on folding of newly-synthesized eEF1A using a yeast cell-free translation system. In this modified version of our previous assay[6], we add cycloheximide to stop further translation at different times after initiation of radiolabeled eEF1A synthesis and assess eEF1A structural integrity by trypsin digestion. In control wild-type extracts, we observed rapid maturation of eEF1A (defined as the trypsin-resistant fraction), but in *aim29*Δ extracts eEF1A matured relatively slowly (Figure 2C). We were able to complement this effect with recombinantly expressed and purified 2xHA-Aim29 protein (Figure 2D) at roughly its physiological concentration as measured by proteomics[28]. Excess Zpr1-3xFLAG supplemented to *aim29*Δ extracts also complemented the eEF1A maturation defect (Figure 2E). In sum, Aim29 shares with Zpr1 all the hallmarks of a genuine eEF1A biogenesis factor, and the defects in *aim29*Δ cells stem from an impaired Zpr1 folding mechanism.

Aim29 recognizes Zpr1 bound to eEF1A in a GTP-bound, pre-hydrolysis state

How might Aim29 facilitate Zpr1-mediated eEF1A folding? To gain insight into a potential physical interaction between Aim29 and Zpr1•eEF1A, we turned to ColabFold[9]. This tool for computationally predicting multimeric protein structures found a relatively high confidence prediction for a Zpr1•eEF1A•Aim29 ternary complex (Figure 3A, S2D–E). The Zpr1/eEF1A interface is largely similar to our previous Zpr1•eEF1A ColabFold model, with minor differences (Figure S2A). Similarly, the Aim29/Zpr1 interface of the ternary complex is akin to the one described in a recent study predicting the existence of Zpr1•Aim29 alongside 105 previously unidentified binary complexes in *S. cerevisiae*[29] (Figure S2B). A striking aspect of the Zpr1•eEF1A•Aim29 model is the conserved region of Aim29 contacting the eEF1A nucleotide-binding motifs, the P-loop and Switch I (Figure S2E). These structural elements allosterically drive GTP hydrolysis-induced conformational changes between domain I and domains II/III during eEF1A's work cycle as a translation elongation factor[7,8].

Examination of many ColabFold Zpr1•eEF1A models (n~500) revealed that some favor the "closed" GTP-bound state of eEF1A where the Switch I helices are nearly perpendicular to each other, while others favor a mixture of "open" GDP-bound states of eEF1A where the Switch I helices unwind into an extended conformation (Figure 3B, S2C)[7,8]. By comparison, all models of Zpr1•eEF1A•Aim29 were in the "closed" GTP-bound conformation, which accordingly yielded a relatively higher confidence score for the switch regions (Figure S2D). This suggested Aim29 selectively recognizes the Zpr1-bound substrate in a GTP-bound, pre-hydrolysis state which we depicted by modeling GTP into our ColabFold model using

AlphaFill[30] (Figure 3A). This idea was appealing because it could explain why our previous proteomics approach, which was not tailored for preserving any nucleotide-sensitive eEF1A interactions, failed to identify Aim29 as a Zpr1-3xFLAG interactor[6]. Thus, we looked for evidence of an interaction by co-IP between Zpr1-3xFLAG and a functional (Figure S3A), 3xHA-tagged version of Aim29 in cell lysates supplemented with nucleotides, and included nucleotides in the subsequent purification steps. While GDP was ineffective, the inclusion of GTP, and even more strikingly, the slowly hydrolyzing GTP-γ-S, enabled persistent Aim29 association with Zpr1-3xFLAG (Figure 3C). Importantly, these nucleotide effects could be reconstituted with purified components (Figure 3D) and further showed stable interaction of Aim29 with Zpr1 was dependent on eEF1A (Figure S3B). These data show Aim29 is minimally sufficient to sense the nucleotide-dependent conformation of the Zpr1•eEF1A folding complex.

eEF1A GTPase activation by Zpr1 is attenuated by Aim29

Our structural modeling suggested eEF1A bound to Zpr1 exists in a variety of conformations that could be produced by an underlying GTP hydrolysis process. To explore this possibility, we turned to our fully-defined *in vitro* system for Zpr1-mediated folding of eEF1A. In this assay, endogenous eEF1A is first purified to homogeneity from its native source and then destabilized by exposure to low glycerol (~5%). We previously reported GTP is required for Zpr1 to convert destabilized eEF1A back into its original trypsin-resistant state, but it was unclear if GTP hydrolysis was occurring[6]. We examined this issue by two orthogonal GTPase assays, one measuring conversion of ^{32}P-labeled GTP to GDP and the other measuring release of inorganic phosphate via an enzyme-linked assay. Strikingly, both revealed Zpr1 stimulated eEF1A GTP hydrolysis in a concentration-dependent manner (Figure 3E and S3C). Three lines of evidence argue GTPase activation by Zpr1 *in vitro* is relevant to eEF1A folding *in vivo*. First, mock-destabilized eEF1A maintained in high glycerol had a relatively negligible basal GTPase activity that was unaffected by Zpr1 (Figure S3D). Second, a structure-guided mutation in Zpr1 (Zpr1^{ZnFMut}), which we previously showed fails to chaperone eEF1A[6], abolished GTPase activation (Figures S3C and S3E). Lastly, our structural modeling predicts that Aim29 recognizes a GTP-bound, pre-hydrolysis conformation of eEF1A that is unfavorable for GTP hydrolysis (Figure S2F and see Discussion). Consistent with this, we observed Aim29 attenuated GTPase activation by ~60% (Figures 3F and S3F). These data suggest Zpr1's chaperone mechanism involves a GTPase cycle; they further imply Aim29 controls the timing of conformational transitions within the cycle.

eEF1A GTP binding and hydrolysis are required for Zpr1-mediated folding

Our data support a working model in which Zpr1-mediated folding requires the client's GTPase cycle. To test the key prediction of this idea using our cell-free assay – that a non-hydrolyzable GTP analog should block folding – we were aided by Zpr1's ability to act post-translationally. Thus, we first synthesized radiolabeled eEF1A in Zpr1-depleted extracts before inhibiting further translation using cycloheximide. Subsequent addition of recombinant Zpr1-3xFLAG led to conversion of ~60% of eEF1A to a trypsin-resistant state within 30 minutes (Figure 4A). Titrating GTP-γ-S into extracts (on top of 100 μM GTP already present in translation reactions) before adding Zpr1 strongly inhibited folding, while

excess GTP or GDP had no effect (Figure 4A and S4A). GTP-γ-S increased the amount of newly synthesized eEF1A that co-immunoprecipitated (co-IP) with Zpr1-3xFLAG after five minutes of Zpr1 addition (Figure 4B), ruling out that GTP-γ-S interferes with Zpr1 substrate recognition. Instead, these data favor a model in which eEF1A's GTPase activity facilitates its release from Zpr1.

We further tested the folding function of eEF1A's GTPase cycle by site-directed mutagenesis. A classic study noted eEF1A's sequence and structural homology to bacterial EF-Tu implicates Asp156 (D156) in the conserved NKXD motif of domain I as the basis of both affinity and selectivity for the guanosine base of nucleotides[31]. Enzymology analysis of eEF1A^{D156N} activity in a poly-Phenylalanine synthesis assay revealed weaker binding to GTP (defined by a higher K_M of mutant relative to wild-type) but a relatively normal synthesis rate at saturating GTP[31]. We also tested the role of GTP hydrolysis by mutating the catalytic His95 (eEF1A^{H95A} and eEF1A^{H95N}) which is coordinated by the ribosome sarcin-ricin loop to initiate attack on the nucleotide gamma phosphate during ribosome-stimulated GTP hydrolysis[32,33]. Mutation of the analogous His84 residue in *E. coli* EF-Tu to alanine slows GTP hydrolysis by orders of magnitude but does not affect binding of EF-Tu•GTP•tRNA ternary complex to ribosomes, nor does it affect the ability of ribosomes to conformationally rearrange upon codon recognition to initiate GTPase activation[34]. Thus, eEF1A^{H95A} is very likely GTPase-dead but still able to bind GTP.

To analyze this panel of eEF1A mutants *in vivo*, we attempted to introduce them into the *tef1*Δ*tef2*Δ double deletion strain (Δ*tef* for simplicity) by standard plasmid shuffling. Not surprisingly, since eEF1A's GTPase activity is expected to be essential for its function as a translation elongation factor, we could not shuffle in plasmids expressing eEF1A^{H95A} and eEF1A^{H95N} (Figure S4D). By contrast, Δ*tef* cells expressing eEF1A^{D156N}-GFP were viable and grew well but had fluorescent punctae indicative of misfolding (Figure 4C). In addition, we found Δ*tef* cells expressing untagged eEF1A^{D156N} had increased eIF2α phosphorylation (Figure 4D), a sign the ISR was constitutively induced. Notably, both eEF1A^{D156N} phenotypes were strongly suppressed by overexpression of Zpr1 (but not Aim29), suggesting that eEF1A GTP binding is required for Zpr1-mediated folding *in vivo* (Figures 4C–D).

In a complementary analysis using the cell-free system, we found eEF1A^{D156N} and eEF1A^{H95N} matured slowly relative to eEF1A^{WT}, while eEF1A^{H95A} folding was severely compromised (Figure 4E). Adding extra GTP to extracts during translation increased the eEF1A^{D156N} maturation rate to nearly eEF1^{WT} rates, but did not rescue the maturation rates of eEF1A^{H95N} or eEF1A^{H95A} (Figure 4E). Finally, co-IP analysis showed all three eEF1A mutants interacted more strongly with Zpr1-3xFLAG, suggesting their maturation defects are not due to inefficient capture by Zpr1 (Fig S4B–C). Taken together, these results demonstrate that eEF1A GTP binding and hydrolysis are jointly required to facilitate eEF1A flux through Zpr1.

Functional coupling between Aim29 and eEF1A GTP binding

The partial nature of the eEF1A^{D156N} folding defect allowed us to uncover additional genetic and biochemical links connecting Aim29 to eEF1A's GTP cycle. First, we

found *aim29*Δ is synthetically lethal with eEF1A^{D156N} (Figure S4E). We also noted that transformation of plasmid-borne eEF1A^{D156N} in *aim29*Δ*tef*Δ cells carrying a second, wild-type eEF1A plasmid resulted in slower growth (Figure S4E). We observed similar dominant negative effects of plasmids expressing eEF1A^{H95A} (severe) and eEF1A^{H95N} (milder) in the *tef*Δ background (Figure S4D) but were unable to obtain the corresponding transformants in the *aim29*Δ*tef*Δ background, which is evidence of a dominant synthetic lethal interaction between the GTPase-dead alleles of eEF1A and the null allele of Aim29. Second, Zpr1-3xFLAG co-IP of 3xHA-Aim29 was abolished following allelic replacement of wild-type eEF1A with eEF1A^{D156N} in the *tef*Δ background, except with partial stabilization by ten-fold higher than normal concentration of GTP-γ-S (Figure S4F). As in the cell-free system, we observed higher Zpr1-3xFLAG co-IP of eEF1A^{D156N} relative to the wild-type eEF1A control in whole-cell extracts (Figure S4F), which could account for the dominant negative effect described above. Indeed, introduction of a plasmid expressing eEF1A^{D156N} into *tef1*Δ cells already expressing Tef1-GFP resulted in aggregation of this otherwise wild-type, second copy of eEF1A (Figure S4G). Lastly, the maturation defect of newly-synthesized eEF1A^{D156N} in cell-free translation extracts was exacerbated in *aim29*Δ extracts (Figure 4F), revealing the biochemical basis of the aforementioned synthetic lethal interaction (Figure S4E). When individually added in excess, 2xHA-Aim29 and GTP achieved partial suppression of the eEF1A^{D156N} folding defect *in vitro*, but in combination they restored folding of this mutant to the level of the wild-type (Figure 4F). In sum, Aim29's function as a Zpr1 co-chaperone is tightly linked to eEF1A GTP binding.

Aim29 and a running GTP cycle drive efficient eEF1A release from Zpr1 in vitro

The Zpr1 co-IP analysis above (Figure 4B, S4B–C) hinted that Aim29 and GTP hydrolysis promote Zpr1•eEF1A dissociation. To characterize this effect, we attempted to reconstitute it using purified components. First, we preformed Zpr1•eEF1A complexes in low glycerol without nucleotides and immobilized them on anti-FLAG beads. Next, we monitored at room temperature the effect of Aim29 and GTP on the appearance of eEF1A in the supernatant fraction over time. Only in the combined presence of GTP and Aim29 was eEF1A release stimulated (~70% in 40 minutes) above an otherwise relatively low background level (Figures 5A–B), and in a concentration-dependent manner (Figure S5A–B). GDP also stimulated release (Figure 5C and S5C), albeit to a lower extent than GTP, but GMP-PNP and GTP-γ-S were ineffective (Figure 5C). Thus, in our minimal biochemical regime, Aim29 and GTP hydrolysis synergistically weaken eEF1A's association with Zpr1.

Structure-function analysis of Aim29's interaction with Zpr1•eEF1A

Finally, we returned to the ColabFold model of Zpr1•eEF1A•Aim29 to validate the predicted structural basis of Aim29's activity as a Zpr1 co-chaperone. We focused our analysis on the highly conserved Aim29 residues in contact with eEF1A's nucleotide switch regions (Figure S2E) and the residues in contact with Zpr1 near the base of its aHH (Figure S2B). We used five assays to measure the effects of alanine mutations targeting Aim29's contacts with the eEF1A Switch I (H53, H97, E133, and E135: Aim29^{SwIMUT}), the eEF1A P-loop (K100: Aim29^{K100A}), or Zpr1 (K40, S41, Y44, R45, N46, W155: Aim29^{ZMUT}) (Figure 6A, S2B, S2E). First, plasmid expression of each Aim29 mutant failed to complement the Hsf1 phenotype of *aim29*Δ cells (Figure 6B, S7A) despite being expressed at similar

levels to the control Aim29^{WT} construct (Figure S6A, S7B). Individual mutations at the SwI- or Zpr1-contacting interfaces only partially complemented and were not further analyzed (Figure S6E–F and S7C–D). Second, Aim29 mutants failed to associate stably with Zpr1-3xFLAG•eEF1A either when isolated from cell extracts or when incubated as purified components (Figures 6C–D and S7E–F). Finally, we detected severely reduced biochemical activity of each Aim29 mutant when we attempted to i) biochemically complement the eEF1A maturation defect of *aim29*Δ extracts (Figure 6E, S7G), ii) dampen Zpr1-stimulated GTP hydrolysis by eEF1A (Figure S6B–D), and iii) stimulate eEF1A release from bead-immobilized Zpr1-3xFLAG (Figure 6F, S7H). In summary, our structure-function analysis argues that Aim29 contacts both components of the Zpr1•eEF1A folding complex as part of its GTPase conformational sensing mechanism.

DISCUSSION

Here we have uncovered the conserved function of Aim29 as a Zpr1 co-chaperone. Unlike Zpr1 genes, which are essential for life across Eukaryotic and Archaeal domains, Aim29 homologs are restricted to Eukaryotes and appear to be absent from certain lineages (plants, nematodes, and insects). Deletion of the Aim29 gene in the budding yeast *S. cerevisiae* results in slow growth (Figure S1E–F) and its deletion in *S. pombe* results in such slow growth (Figure S1J) that effectively renders it an essential gene. Genome-wide screening in *S. cerevisiae* previously defined *aim29*Δ as the top Hsf1 “stressor” allele within the uncharacterized gene category[35]. We can now say this top ranking is the result of massive misfolding of eEF1A, one of the most abundant cellular proteins[28], because Zpr1 cannot work efficiently without Aim29. Our evidence suggests Hsf1 prevents proteostasis from collapsing in *aim29*Δ cells by mitigating eEF1A misfolding, lest it result in severe growth arrest (Figure S1A). We also found the essentiality of Aim29 in *S. pombe* can be robustly bypassed by Zpr1 overexpression or a Zpr1 gain-of-function mutation (Figure S1J–K). It remains to be determined if the role of Aim29 was bypassed in certain eukaryotic lineages by positive selection on Zpr1, or if its absence became effectively tolerated by eEF1A proteostasis.

We propose Zpr1-mediated folding requires an eEF1A GTPase cycle and conformational sensing by Aim29, which together facilitate Zpr1 recycling (Figure 7). This model provides an explanation for our *in vivo* observations. First, it explains the ability of Zpr1 overexpression to restore eEF1A folding and function in cells lacking Aim29 or expressing eEF1A^{D156N}, a mutant with a GTP-binding defect (Figures 2A–B, and 4C–D). Second, it explains why eEF1A^{D156N} showed enhanced interaction with Zpr1 *in vivo* but a reduced ability to recruit Aim29 to the folding complex (Figure S4F). Third, it rationalizes how eEF1A^{D156N} could bring about the observed aggregation of a wild-type copy of eEF1A (Figure S4G) in the same cells by dominantly “clogging” client flux through Zpr1. The same mechanism of flux interference is sufficient to explain other dominant negative growth effects observed by our study (Figures S4D–E). Cell-free analysis provided biochemical support for these genetic interactions and enabled us to further validate the model with GTP cycle perturbations. First, we found a strong defect of eEF1A maturation to the trypsin-resistant state in the presence of non-hydrolyzable GTP analogs or when we ablated the catalytic His95 of eEF1A required for GTP hydrolysis (Figures 4A,E and S4A).

Second, newly-synthesized eEF1A accumulated in a Zpr1-bound state when we disrupted the GTPase cycle in several ways (Figures 4B and S4B–C). Lastly, we reconstituted eEF1A conformational sensing by Aim29 using purified components and observed eEF1A's association with Zpr1 weakened in the presence of Aim29 and GTP (Figures 3D, 5A–B, and S5A–B). This latter reaction occurred less efficiently in the presence of GDP and was blocked by non-hydrolyzable GTP analogs (Figures 5C and S5C).

Further support for our model comes from measurements of eEF1A's GTPase activity. Namely, Zpr1 robustly awakened GTP hydrolysis by eEF1A that was first purified as a native protein but then destabilized *in vitro* (Figures 3E and S3C). The detailed enzymology of this process remains to be determined but ColabFold provides a potential structural glimpse into its mechanism. Unlike a typical GTPase activating protein (GAP), Zpr1 is not predicted to stimulate hydrolysis by catalytic residue complementation. Instead, modeling of Zpr1 binding to eEF1A yielded a distribution of conformational switch-region states resembling "closed" GTP-bound and a mixture of "open" GDP-bound solved eEF1A structures (Figures 3B, S2C). A hypothetical allosteric basis for these conformational dynamics can be derived from an analogous mechanism in which the kirromycin family of antibiotics induces GTPase activation of bacterial EF-Tu[36–38]. Both methyl-kirromycin and the ZnF, which is required for Zpr1's GAP activity (Figure S3C,E), intercalate into the hydrophobic interface between domain I and domain III of their homologous targets[6,39]. ColabFold also suggests a plausible structural basis by which Aim29 reduces the GTPase activity of Zpr1•eEF1A. His95 of eEF1A is thought to function as a general base to facilitate attack of the γ-phosphate of GTP by a catalytic water molecule[32,33,40,41]. In Zpr1•eEF1A models containing Aim29, we see stabilization of an unfavorable His95 conformation and closure of the nearby "hydrophobic gate" through which the attacking water molecule enters the active site (Figure S2F). This view resembles the proposed mechanism by which the archaeal translation termination factor aRF1 arrests aEF1A GTP hydrolysis before stop codon recognition[40] (Figure S2F). Experimental testing of this prediction will be facilitated by structural analysis of a Zpr1•eEF1A•Aim29•GTP-γ-S quaternary complex.

We are reluctant to speculate about the structural basis by which Aim29 appears to couple GTP hydrolysis to eEF1A release from Zpr1. It is intriguing, however, that Aim29 is predicted to contact Zpr1 at the nexus of the C-terminal ZnF and aHH that somehow work together to enable eEF1A folding[6]. We have found a Zpr1 gain-of-function mutation near this interface that bypasses Aim29's function across two highly divergent yeast species (Figure S1K–L). This mutation might affect a Zpr1 allosteric network that transduces Aim29's activity as a mechanical coupling device. Another related question is whether additional cellular factors promote Zpr1 recycling by providing a "sink" for released eEF1A. One top candidate is the eEF1A nucleotide-exchange factor, eEF1B, which is present at approximately 10-fold higher concentration than Zpr1 (PaxDb)[28] and was previously shown to bind eEF1A in competition with Zpr1[42]. The ability to reconstitute eEF1A folding using our post-translational cell-free assay will facilitate efforts to isolate additional eEF1A biogenesis factors.

From a broader protein folding perspective, a role for GTP binding in the biogenesis of G protein α-subunits (Gα) has been noted. Following complex formation with the

Ric-8 chaperone, a Gα client becomes poised to interact with GTP, which upon binding induces dissociation of the chaperone-client complex without a requirement for GTP hydrolysis[13–16]. In a second example involving dimeric tubulin, late stages of folding and assembly depend on GTP hydrolysis by a GTPase, Arl2, which facilitates the final alpha/beta tubulin dimerization step[43]. The potential role of a client GTPase cycle in the context of two other specialized G protein folding mechanisms, eEF2 biogenesis[44,45] and eIF2 assembly (a trimeric complex containing an eEF1A-like subunit)[46,47], has not to our knowledge been explored but should be considered in light of our findings. Lastly, we have placed eEF1A folding into an unexpected juxtaposition with Hsp90 and its co-chaperone p23. p23 modulates a conformational folding cycle in two ways similar to Aim29. First, it senses a specific ATP-bound Hsp90 state and causes a conformational change in the ATPase active site of the middle domain to inhibit hydrolysis[48]. Second, it directly interacts with a model client protein, the glucocorticoid receptor (GR), to enhance its ligand-binding activity and enable its dissociation in the presence of hormone[48,49,50]. Future work comparing these two parallel systems will offer new insight into the fundamental role of nucleotide-driven conformational changes in protein folding.

Limitations of the study

We have established eEF1A biogenesis requires a GTPase folding cycle, which is conformationally sensed by Aim29 acting as a Zpr1 co-chaperone. However, we lack a full mechanistic understanding of how GTP hydrolysis and Aim29 bring about the disassembly of the Zpr1•eEF1A folding complex. Our biochemical reconstitution of this process now paves the way towards structural and FRET-based studies of the underlying eEF1A domain rearrangements. Finally, a thermodynamic and kinetic framework for describing our in vitro chaperone system awaits future measurements of equilibrium and rate constants for each step in the cycle.

STAR METHODS

RESOURCE AVAILABILITY

Lead Contact—Further information and requests for resources or reagents should be directed to the lead contact, Vladimir Denic (vdenic@mcb.harvard.edu).

Materials Availability—The plasmids and yeast strains generated in this study may be requested from the lead contact.

Data and code availability

- Raw RNA-sequencing data has been deposited in the GEO database and is available under accession number GSE229425. Ribo-seq data has been deposited in the GEO database and is available under accession number GSE229777.
- This paper does not report original code.
- Any additional information required to reanalyze the data reported in this paper is available from the lead contact upon request

EXPERIMENTAL MODEL AND SUBJECT DETAILS

Yeast Strains—All strains used in this study are listed in the key resources table. Cells were cultured on solid agar plates or in liquid media unless otherwise indicated.

METHOD DETAILS

Plasmids—All plasmids used in this study are listed in the key resources table.

Yeast strain construction

Stable genome modifications: PCR-mediated gene deletion and gene tagging was carried out as described elsewhere[51]. Lithium acetate-mediated transformation was done as described elsewhere[52]. Gene deletions were done using the following primers (found in the Key Resources Table) to generate deletion cassettes with homology arms to the indicated locus: *aim29*Δ: oVD11404 and oVD11405; *tef2*Δ: oVD12116 and oVD12117; *tef1*Δ: oVD13227 and oVD13229 for homology to 3'UTR of *TEF1*, oVD13228 and oVD13231 to amplify the *natMX* cassette, and oVD13230 and oVD13232 to amplify the 5' UTR of *TEF1*.

tefΔ strains: The *TEF2* gene was deleted from its endogenous locus using a *HIS3* cassette to generate VDY6184. VDY6184 was subsequently transformed with either pVD2748 (WT *TEF2*) or pVD2749 (S53A *TEF2*) to generate VDY6272 and VDY6273, respectively. The *TEF1* gene was deleted from its endogenous locus in VDY5662 using a *natMX* cassette to generate VDY6269. VDY6269 was subsequently crossed to VDY6272 and sporulated to obtain strains VDY6281 and VDY6282. VDY6269 was crossed to VDY6273 and sporulated to retrieve strain VDY6279. Strains lacking both copies of eEF1A were unable to grow on media containing 5-fluoroorotic acid (5-FOA) due to counterselection of the necessary rescuing plasmid containing either $TEF2^{WT}$ *or* $TEF2^{S53A}$.

eEF1A and Zpr1 plasmid shuffles—All *tef*Δ strains (*tef1*Δ *tef2*Δ) used for plasmid shuffles and the URA3-based pRS416-*PrTEF2-TEF2* plasmids they harbor are listed in the Key Resources Table. pRS series vectors are described elsewhere[53]. These strains were transformed with TRP1-based pRS414-*PrTEF2-TEF2* variants as indicated in figures and transformants were selected on SD -Trp media. Individual transformants were struck on SD -Trp plates and allowed to grow for an additional 48 hours. Cells were then struck on SD + 5-FOA plates and allowed to grow for 2-3 days to counter-select against the pRS416 URA3-based plasmid.

All *zpr1*Δ strains and the URA3-based pRS416-*PrZPR1-ZPR1* plasmids they harbor are also listed in the Key Resources Table. They were treated similarly to *tef*Δ strains described in the paragraph above, but with the TRP1-based pRS414-*PrZPR1-ZPR1* variants as indicated in figures.

Antibodies—For immunoblotting, primary antibodies were used at the indicated dilution and secondary antibodies were used 1:3,000 (HRP) or 1:10,000 (fluorescent). Primary antibodies include the following: rabbit-anti-eEF1A ([1:10,000 - IB], ED7001, Kerafast Inc., Boston, MA), rabbit-anti-EIF2S1 phospho S51 (eIF2α phospho Ser51) ([1:1000 - IB],

ab32157, Abcam), mouse-anti-FLAG M2 ([1:2000-1:5000 - IB], F3165, MilliporeSigma, Burlington, MA), mouse-anti-PGK1 ([1:2000 - IB], 459250, Thermo Fisher Scientific, Waltham, MA), rabbit-anti-Hexokinase ([1:2000 - IB], U.S. Biological Life Sciences, Swampscott, MA), rat-anti-HA ([1:2000-1:5000 - IB], Roche, Basel, Switzerland), mouse-anti-ZPR1 monoclonal antibody ([1:500-1:1000 - IB], Thermo Fisher Scientific, Waltham, MA). Immunoprecipitations using the mouse-anti-FLAG M2 antibody were performed as described in "Immunoprecipitations" below.

Immunoblotting—Yeast cell lysates were prepared as follows. Equal OD_{600} amounts of cells in mid-log phase were collected, rinsed in PBS, and resuspended in SDS/urea sample buffer (20 mM Tris-HCl pH 6.8, 4 M Urea, 2.5% SDS, 0.05 mM EDTA, 1% Beta-mercaptoethanol, 10% glycerol). Acid-washed 0.5 mm glass beads were added to cell suspensions and subjected to bead beating at 4°C for 1-2 minutes using a Biospec Products bead beater. Samples were then heated to 100°C for 5 minutes followed by centrifugation for 5 minutes at 20,000 x g to pellet insoluble material, and supernatants were analyzed.

Samples were separated via SDS-PAGE and transferred to nitrocellulose before blocking with 5% skim milk in TBST (50 mM Tris-HCl pH 7.4, 150 mM NaCl, 0.1% Tween 20, 0.25 mM EDTA) for 45-60 minutes. Membranes were probed with primary antibodies overnight at 4°C with antibody dilutions indicated in the Antibodies section. After three rinses in TBST, membranes were probed with secondary antibodies at dilutions indicated in the Antibodies section. HRP-conjugated antibodies were visualized using Super Signal West Femto (Thermo Fisher Scientific). Fluorescent secondaries were visualized on a LI-COR Odyssey scanner. Quantification of band intensity was done using ImageJ.

Autoradiography—Protein samples were separated via SDS-PAGE. Gels were fixed for 30 minutes in fixing solution (50% methanol and 10% acetic acid) and then rinsed for 30 minutes in drying solution (30% methanol and 5% glycerol) before drying under vacuum for 2 hours at 80°C. Phosphor screens (GE Healthcare) were exposed to dried gels overnight and then scanned on a Sapphire Biomolecular Imager (Azure Biosciences). Quantification of band intensity was done using ImageJ.

For GTPase assays, phosphor screens were exposed to dried PEI-cellulose plates (run as described in the GTPase Assays section below) for 30-60 minutes before scanning on a Sapphire Biomolecular Imager (Azure Biosciences). Quantification of spot intensity was done using ImageJ.

Flow cytometry—For measurement of Hsf1 activity, strains VDY3334, VDY5662 and VDY5849 carrying the 4xHSE-YFP reporter integrated into the genome [23] were transformed with empty vector (pVD2878) or the indicated low-copy Aim29 plasmid (pVD1895, pVD1899, pVD2204 or pVD2822). Cells were grown to saturation overnight in synthetic defined media (SD - Ura) with 2% dextrose and back-diluted to an OD_{600} of 0.1 the next day and grown for 4.5 hours until an OD_{600} ~0.5 was reached. Hsf1 activity for respective strains was subsequently measured using a FACSymphony A3 analyzer (BD Biosciences) using the 488 nm laser (FITC channel). 10,000 cells were measured for each sample and

medians/histograms were collected using the R packages flowCore and flowViz and plotted using ggridges (see Key Resources Table for software information).

For measurement of Gcn4 activity, a Gcn4 reporter consisting of the 4 upstream ORFS in 5' UTR region of *GCN4* driving the expression of GFP on a high-copy plasmid (a kind gift from Onn Brandman; named pVD2746 in this work) was transformed into VDY465, VDY5670 and VDY5851. Cells were grown to saturation overnight in synthetic defined media (SD - Ura) with 2% dextrose and back-diluted to an OD_{600} of 0.1 the next day and grown for 4.5 hours until an OD_{600} ~0.5 was reached. For the amino acid starvation control (VDY465 + pVD2746), after overnight growth and back-dilution as for the other strains, cells were grown for an hour in synthetic defined (SD) media with 2% dextrose without amino acids prior to collection for flow cytometry. Gcn4 activity was measured using a FACSymphony A3 analyzer (BD Biosciences) using the 488 nm laser (FITC channel). 10,000 cells were measured for each sample and medians/histograms were collected using the R packages flowCore and flowViz and plotted using ggridges.

Growth Curve Assays—VDY3334, VDY5662, VDY5849 (Figure S1F) or VDY3334, VDY6293, VDY6295, VDY6297 (Figure S1E) were grown to mid-log phase before back-dilution to an OD_{600} of 0.1 in 200 μL of synthetic complete media, in 96-well plates. Cells were grown for 24 hours with continuous shaking at 30°C with OD_{600} measurements taken every 10 minutes. VDY6300, VDY6301, VDY6302 and VDY6303 (Figure S1A) were grown to mid-log phase in synthetic defined media (SD -Trp) at room temperature and inoculated at OD_{600} 0.1 in 200 μL of SD -Trp media in a 96-well plate covered with BreatheEasy sealing membranes (Sigma-Aldrich). Cells were grown for 24 hours with continuous shaking at 25°C with OD_{600} measurements taken every 10 minutes. All experiments were done in triplicate and the mean of these samples was used to produce the final plot.

Microscopy

Hsp42-mCherry/Tef1-GFP aggregation assay: Isolates of VDY6230 or VDY6231 transformed with empty vector (pVD13) and VDY6231 transformed with pVD2323 were grown to saturation overnight in synthetic complete (SC) media containing 2% dextrose. Cells were back-diluted to an OD_{600} of 0.1 in SC + 2% dextrose and grown for 4.5 hours to reach an OD_{600} ~0.5 prior to imaging. For Figure 4C, pVD2900 or pVD2901 were shuffled in as the only copy of *TEF2* into the *tef*Δ strain (VDY6282) and these strains were subsequently transformed with pVD1967, pVD2891, or empty vector. These strains were then grown to saturation overnight in synthetic defined media (SD -Ura) and then back-diluted to an OD_{600} of 0.1 in SD -Ura and grown for 4.5 hours to reach an OD_{600} ~0.5 prior to imaging. Cells were imaged with a 100x objective (NA = 1.42) on a Nikon TI inverted microscope using a Yokogawa dual spinning disk confocal unit and a Hamamatsu ImagEM EM-CCD camera. Images were acquired using MetaMorph software. A 488 nm laser with a Semrock FF01-525/45 emission filter was used for imaging GFP and a 594 nm laser with a Semrock FF01-609/57 for mCherry fluorescent protein. 0.5-micron slices with a total depth of 10 microns were used for z stack acquisition. Maximum intensity z-projections were used to generate the final images from collected z stacks.

RNA-seq—Three isolates each of VDY3334, VDY5662, and VDY5849 were grown to mid-log phase in YPD. When cells reached OD_{600} 0.4-0.6, 1 OD_{600} unit was collected for RNA isolation by rapid centrifugation for 1 min at 20,000 x g. A separate aliquot of each culture also containing 1 OD_{600} unit was also collected for immunoblotting analysis as described in the "Immunoblotting" section. Cell pellets were snap frozen in liquid nitrogen and stored at −80°C until sending to Azenta Life Sciences (Chelmsford, MA, USA) for isolation of total RNA, polyA enrichment, and sample QC before preparation of Illumina sequencing libraries for paired-end sequencing using an Illumina HiSeq. Each point in Figure 1B and Supplemental Figure S1I denotes a gene, where the gene abundance Z-score is obtained by gene-wise mean centering and scaling to the standard deviation across all timepoints using degPatterns (see Key Resources Table for software information).

Preparation of Ribo-seq libraries—VDY3334 and VDY5662 were grown in 800 mL YPD to OD_{600} of 0.4-0.5 and then rapidly filtered using a vacuum filtration apparatus (less than 60 seconds filtration time) and flash frozen in liquid nitrogen. Isolation of ribosome-protected footprints and generation of libraries for Illumina sequencing is described in great detail elsewhere [54].

Genetic screening in *S. pombe*

Overexpression screen: Starting with pREP *nmt1 LEU2* (a kind gift from D. Moazed's lab) we used standard isothermal assembly approaches to sequentially insert the following elements: 1) *aim29*$^+$ ORF into a MCS flanked by the *nmt1* promoter and terminator; 2) *ura4*$^+$ locus, which effectively replaced most of *LEU2*; 3) *ade6*+ locus. The resulting plasmid, pREP *ura4*$^+$ *ade6*$^+$ P_{nmt1}-*aim29*-T_{nmt1} (pVD2145) enabled a BOE screening approach described below.

To create the *S. pombe* strain suitable for isolation of *aim29*Δ BOE suppressors, we used standard yeast transformation to first introduce pREP *ura4*$^+$ *ade6*$^+$ P_{nmt1}-*aim29*-T_{nmt1} into the SPY76 genetic background (*h*$^+$ *leu1-32 ade6-M216*). The *aim29*$^+$ locus in the resulting strain was then knocked out using an *aim29::kan*^{R} resistance cassette with long homology arms. The resulting VDY5838 strain was validated by colony PCR, inability to grow on media containing 5-FOA (cf. parental strain), and absence of colony sectoring from white to red on media with low adenine (cf. parental strain). For further validation, we transformed VDY5838 with either empty pREP nmt1 LEU2 or containing *aim29*+ ORF but could only achieve plasmid shuffling with transformants of the latter.

The two *S. pombe* cDNA libraries that we used were under the control of the *adh* promoter and actin terminator; they differed from each other in average length (SPLE-1 and SPLE-2)[55] of inserts into the pLEV3 backbone. Following high-efficiency transformation into VDY5838, transformants were plated onto multiple EMM-LEU plates. We screened approximately 28,000 transformants for each library by replica plating onto YES 5-FOA plates. After 2 days incubation at 32°C, each library was replica plated again onto YES 5-FOA low adenine plates. Following an additional 2 days of incubation at 32°C and another 3 days at 4°C (to facilitate red pigment accumulation), we found strong BOE suppressors by their appearance as large red colonies. To recover cDNA plasmids after colony purification

on fresh YES 5-FOA low adenine plates, we grew the suppressors to saturation in liquid YES media. Following the standard “smash and grab” procedure for yeast plasmid recovery, we electroporated the extracted nucleic acids into DH5α cells. Plasmids from the resulting Amp^R transformants were miniprepped and Sanger sequenced to determine the identity of their inserts. In both libraries, we repeatedly found hits only in *aim29*$^+$ and *zpr1*$^+$. The recovered *zpr1*$^+$ plasmids were able to re-confer the BOE suppressor phenotype upon re-transformation into VDY5838. We also recapitulated this phenotype using a pLEV3 plasmid carrying a distinct *zpr1* ORF insert, which we amplified de novo from genomic DNA.

UV mutagenesis screen to isolate bypass of essentiality suppressors of aim29Δ: VDY5838 was grown in YES media overnight to saturation. On the next day, 10^7 cells were plated onto YES + 5-FOA media containing low amounts of adenine (low Ade). Using the Stratagene UV Stratalinker 2400, cells were irradiated with UV (40 mJ/cm^2). Cells were allowed to grow for five days at 32 °C. To remove background, cells were replica plated onto YES + 5-FOA media (low Ade) and allowed to grow for two more days before picking red colonies. Whole genome sequencing to identify suppressor mutations was performed as described for *S. cerevisiae* in Koschwanez et al., 2013 [56].

Tetrad analysis: *S. pombe* strains VDY5803 and VDY5819 or VDY5878 (each an independently isolated BOE suppressor encoding *zpr1-T353I*) were mated overnight at RT on SPA plates. Diploid cells were picked and allowed 24-48 hours to sporulate. Tetrads were scraped off of SPA plates and resuspended in water before being plated onto YES media. Tetrads were picked and allowed to grow for four days before imaging.

Spotting Assays—VDY5838 was transformed with pVD2914 (Figure S1J), pVD2042 (Figure S1J–K) or pVD2184 (Figure S1O). After initial selection on solid EMM-Leu media individual isolates were struck on fresh EMM-Leu solid media for 48 hours to allow loss of plasmids containing *ura4*$^+$ *ade6*$^+$ selection markers. Cells grown to mid-log phase in liquid EMM-Leu media were then back-diluted to an OD_{600} of 0.5 and spotted in a serial dilution series (1:10) on EMM-Leu or EMM -Leu +5-FOA (low Ade) plates and grown at 30°C for 96 hours before imaging.

Immunoprecipitations

Zpr1-3xFLAG from cell lysates: VDY465 and VDY6197 transformed with empty vector or pVD2871 (Figure 3C) were grown in 1L cultures to OD_{600} 1.8 in liquid SD -Ura media. For the experiments in Figure 6C, we used VDY6197 transformed with pVD2872 or pVD2873. For Figure S4F, *tef*Δ *ZPR1-3xFLAG pRS416-PrTEF2-TEF2*^{S53A} cells (VDY6279) with pVD2858 or pVD2860 shuffled in were subsequently transformed with pVD2871 before growth and collection.

Cells were spun down at 3500 x g for 15 minutes at 4°C, washed in 50 mL ddH2O twice and resuspended in 1 mL per gram of pellet of resuspension buffer (1.2% PVP-40, 20 mM HEPES pH 7.4, 1x protease inhibitor cocktail [Roche] , 1% solution P [2 mg Pepstatin A, 90 mg PMSF, 5 mL 100% ethanol], 1 mM DTT).Cells were spun down at 3500 x g for 15 minutes to remove all buffer. Cell paste was placed into a syringe and was pushed out to

be frozen as “noodles” in a 50 mL conical tube filled with liquid nitrogen. Liquid nitrogen was decanted from the tube and frozen “noodles” were stored at −80°C until cryogenically lysed using a Retsch PM100 ball mill. 250 mg of powder was thawed at 4°C followed by resuspension in 1 mL of HIP buffer (40 mM HEPES-KOH pH 7.5, 110 mM KOAc, 2 mM $MgCl_2$, 1% Triton X-100, 0.1% Tween, 1x protease inhibitor cocktail [Roche], 1% solution P, 1mM DTT) supplemented with 100 μM GTP, GDP or GTP-γ-S where indicated. Lysate was passed through a Whatman 25 mm GD/X Disposable filter (Cat No. 6888-2527). Equal volume of lysates was added to 62.5 μL Protein G dynabeads pre-bound to 3.75 μL of anti-FLAG M2 antibody and agitated for 30 minutes at 4°C. Beads were washed briefly for 30 seconds 1x in HIP buffer. After the final wash, protein was eluted from beads with two pooled incubations of 15 μL 1 mg/mL 3xFLAG peptide in HIP buffer supplemented with the indicated nucleotides at room temperature for 15 min. Samples were analyzed via SDS-PAGE and immunoblotting.

Purified Zpr1-3xFLAG with eEF1A and 2xHA-Aim29: Pure eEF1A was diluted in Buffer A (20 mM HEPES pH 7.4, 100 mM KoAc, 2 mM $Mg(OAc)_2$, 2mM DTT) with 5% glycerol for 10 min alone at 2x the final concentration. Zpr1-3xFLAG and nucleotide (if present) was added for 10 min and either buffer or 2xHA-Aim29 was added for a final 30 min so that the final concentration of each protein was 3 μM and nucleotide was 1 mM. An aliquot was removed as the total. Samples were added to Protein G Dynabeads pre-conjugated to anti-FLAG antibody (~1 μL antibody per 16.6 μL beads) resuspended in 1 reaction volume of Buffer A with 5% glycerol. Samples were agitated at 4°C for 30 min, unbound material was removed and samples were washed 3x in 1 mL cold wash buffer (Buffer A with 5% glycerol and 0.05% Tween). Samples were eluted after agitating for 30 min at RT with 1 mg/mL 3xFLAG peptide in Buffer A with 5% glycerol. Equal amounts of totals and IPs were added to 2x SDS/Urea sample buffer (20 mM Tris-HCl pH 6.8, 4 M Urea, 2.5% SDS, 0.05 mM EDTA, 1% Beta-mercaptoethanol, 10% glycerol), heated at 80°C, and analyzed by SDS-PAGE and Coomassie staining.

Co-immunoprecipitation of radiolabeled eEF1A folding intermediates with Zpr1-3xFLAG: Translation reactions were assembled and translated as described in “Post-translational eEF1A trypsin resistance assays”. After cycloheximide treatment extracts were treated with nucleotides or water (for mock “-” treatments) where indicated. Approximately one minute following nucleotide addition, recombinantly expressed and purified Zpr1-3xFLAG was added to extracts to 1 μM to initiate the eEF1A maturation reaction. After 5 minutes of incubation with Zpr1-3xFLAG the reaction mixtures were moved to ice. Protein G Dynabeads conjugated to mouse-anti-FLAG M2 antibody were resuspended in the reaction and incubated at 4°C for 20 minutes in a thermomixer at 1400 RPM. Beads were rinsed 1x with ice cold buffer ADG with 0.01% Triton X-100 and moved to new tubes. Beads were heated to 80°C for 5 minutes in SDS/Urea sample buffer to elute immunoprecipitated complexes. Samples were analyzed via SDS-PAGE and autoradiography.

eEF1A release assays: For release assays to monitor eEF1A dissociation from Zpr1-3xFLAG, the following changes were made: reactions were set up so that the final

concentration of eEF1A and Zpr1 would be ~150 nM and 300 nM respectively in 24 μL after splitting the washed beads into 25 tubes. 1 sample was set aside, and the remaining 24 were incubated in 24 μL Buffer A + 5% glycerol with the indicated added components for the indicated times at RT with agitation. Supernatant was removed, and the beads for all 25 samples were eluted with 24 μL 1 mg/mL 3xFLAG peptide in Buffer A + 5% glycerol as before. Equal amounts of supernatant and eluate from the beads were added to 2x SDS/Urea sample buffer, heated at 80°C, and analyzed by SDS-PAGE and immunoblotting.

Lgt3 glucosylation assay—VDY3334, VDY5662, VDY5849, and VDY5850 transformed with pRS414 CEN/ARS plasmids (either empty vector ["E.V."; pVD2766] or with *AIM29* under its endogenous promoter ["p*AIM29*"; pVD1898]) were grown in synthetic media (SD - Trp) to OD_{600} 0.4-0.6 (mid-log phase) in 50 mL cultures and collected via centrifugation at 5,000 x g for 3 minutes at 4°C. All subsequent extract preparation steps were performed at 4°C. Pellets were resuspended in 1 mL ice cold PBS and transferred to pre-weighed 1.5 mL tubes. Cells were centrifuged at 20,000 x g for 1 min and then all supernatant was removed. Pellets were weighed and a volume of ternary complex lysis buffer (30 mM HEPES pH 7.5, 100 mM KOAc, 2 mM $Mg(OAc)_2$, 25% glycerol, 1x protease inhibitor cocktail [Roche]) equal to the pellet weight (1 mL buffer per 1 g pellet) was added. Cell suspensions were subjected to bead beating for 60 seconds and subsequently placed on ice for 2 minutes. The tubes were punctured at the bottom and spun at 1000 x g for 1 minute into 15 mL conical tubes. The crude lysate was clarified by centrifugation at 16,000 x g for 10 min at 4°C. The supernatant was aliquoted into single-use aliquots, snap frozen in liquid nitrogen, and stored at −80°C.

Reactions for eEF1A ternary complex glycosylation contained 3.3 μl crude extract, 0.5 μl of 20 μM recombinant Lgt3 (1 μM final), 0.6 μl of 333 μM ^{14}C-UDP-glucose (20 μM final; uniformly labeled, American Radiolabeled Chemicals Inc.) and 5.6 μl ternary complex lysis buffer. Reactions were set up on ice and moved to a thermomixer (Eppendorf) at 25°C and 1200 RPM to initiate the reaction. After 5 minutes of incubation, 10 μl of 2x SDS/Urea sample buffer was added and samples were incubated at 80°C for 5 minutes. Samples were analyzed via SDS/PAGE and autoradiography or immunoblotting for the indicated proteins.

Yeast *in vitro* transcription and translation

Generation of capped mRNA: Capped mRNAs were *in vitro* transcribed from the appropriate PCR products using the mMESSAGE mMACHINE T7 kit (Invitrogen) as described previously [57]. PCR products encoding *TEF2* variants were generated from pVD2858 (*TEF2*), pVD2860 ($TEF2^{D156N}$), pVD2904 ($TEF2^{H95A}$), or pVD2906 ($TEF2^{H95N}$) using the primers oVD13102 and oVD13103.

Preparation of cell-free translation extracts: Cell-free translation extracts were prepared as previously described [6]. First, 1.5 L YPD media was inoculated with the indicated strains (VDY3334 [WT] or VDY5662 [*aim29*Δ]) at OD_{600} 0.1 and grown to OD_{600} 1.8-2.0. Cells were collected via centrifugation at 3,000 RPM in a JS-4.2 rotor for 15 minutes at 4°C. Cells were rinsed once in cold DEPC-treated water and then once in cold Buffer A (20 mM HEPES pH 7.4, 100 mM KoAc, 2 mM $Mg(OAc)_2$) plus 2 mM DTT. Cells were mixed with

1 mL Buffer A with 2 mM DTT, 14 % glycerol (Buffer ADG), and 2x complete protease inhibitor cocktail (PIC) tablet (Roche, Basel, Switzerland) per 6 grams of cell weight. Cell paste was then frozen in liquid nitrogen drop by drop, lysed in a Retsch PM100 ball mill, and stored at −80°C. Powder was thawed at 4°C followed by addition of 2 mL Buffer ADG + PIC. Thawed lysate was then centrifuged at 13,336 x g for 10 minutes at 4°C. Supernatant was centrifuged at 49,000 RPM in a SW-55 rotor for 30 minutes at 4°C and the clear supernatant was taken while avoiding the upper lipid layer. The collected supernatant was run over five sequential Hi-Trap desalting columns (GE Healthcare, Chicago, IL, USA) on an AKTA Pure FPLC system. Fractions with A_{260} > 50 were pooled and snap frozen in liquid nitrogen. Before translation reactions, all translation extracts were treated with 2.4 µL 40 mM CaCl2 and 1 µL micrococcal nuclease (NEB) per 200 µL extract for 10 minutes at room temperature followed by treatment with 3.6 µL 100 mM EGTA for 5 minutes.

Co-translational eEF1A trypsin resistance assays: Reactions for eEF1A trypsin protection time courses in Figure 2 were performed in 15 µL total volume per time point and contained the following components: 2.5 µL 6x translation buffer (132 mM HEPES-KOH pH 7.4, 720 mM KOAc, 9 mM $Mg(OAc)_2$, 4.5 mM ATP, 0.6 mM GTP, 150 mM creatine phosphate, 0.24 mM each amino acid but lacking methionine, 10.2 mM DTT), 0.5 µL Riboguard RNAse inhibitor (Lucigen), 0.5 µL 20 mg/mL creatine kinase, 1 µL of 200 ng/µL capped mRNA, 1 µL of ^{35}S-Methionine (10 mCi/mL; Perkin Elmer), 1 µL of 15x 2xHA-Aim29 or Zpr1-3xFLAG recombinant protein or buffer (Aim29: 50 mM Tris pH 7.5, 200 mM NaCl, 10% glycerol, 0.5 mM TCEP; Zpr1: 50 mM Tris pH 8.0, 200 mM NaCl, 10% glycerol, 0.5 mM TCEP), and 8.5 µl of nuclease-treated extracts. Reactions were incubated at room temperature and at the indicated times aliquots were removed for one of two treatments: (1) to prepare “before trypsin” samples to determine total eEF1A translated at each time, 5 µL was plunged into SDS-Urea sample buffer (20 mM Tris-HCl pH 6.8, 4 M Urea, 2.5% SDS, 0.05 mM EDTA, 1% Beta-mercaptoethanol, 10% glycerol) and heated to 80°C for 5 minutes to quench translation; (2) to prepare “after trypsin” samples, 10 µl of the reaction was added to a tube containing 1.25 µl of 1 mg/ml cycloheximide and 1.25 µl of 0.5 mg/ml trypsin, mixed thoroughly by pipetting, and incubated at room temperature for 5 minutes before quenching in 7.5 µl of 2x SDS-Urea sample buffer and heating to 80°C for 5 minutes. Equal amounts of both “before trypsin” and “after trypsin” samples were analyzed by SDS-PAGE and autoradiography. Only “before trypsin” samples were analyzed by SDS-PAGE and immunoblotting. Reactions in Figure 2D–E were only analyzed after 15 minutes of translation. Reactions in Figure 4E–F were performed similarly but contained *TEF2* mutant mRNA, 500 nM 2xHA-Aim29, and/or additional GTP to final 1 mM as indicated in the figures. Reactions in Figure 6 were performed as in Figure 2.

Post-translational eEF1A trypsin resistance assays: Reactions in Figure 4A and S4 were assembled as in co-translational assays but in Zpr1-depleted extracts derived from *ZPR1-AID* cells treated with 5 µM 5-Ph-IAA as previously described[6]. After translation at 25°C for 30 minutes cycloheximide was added to 100 µg/mL final concentration to inhibit further translation. Two aliquots were removed to monitor the eEF1A trypsin resistance in the absence of Zpr1: one was immediately added to to SDS/urea sample buffer and the other was first treated with 50 µg/mL trypsin for 5 minutes before quenching in SDS/urea

sample buffer. Next, nucleotides or water (for mock treatments) were added to extracts where indicated. Approximately one minute following nucleotide addition, recombinantly expressed and purified Zpr1-3xFLAG was added to extracts to initiate the eEF1A maturation reaction. Aliquots were removed at the indicated times and subjected to a 5 minute trypsin digest as described above before quenching with SDS/urea sample buffer. At the end of the time course an additional aliquot was placed directly into SDS/Urea sample buffer without being subjected to trypsin digestion and analyzed to ensure that translation had been effectively inhibited. All samples were analyzed by SDS-PAGE and autoradiography. Densitometry to quantify band intensity was done as described under “Immunoblot and autoradiography quantification”. Fraction resistant is the signal of trypsin-resistant eEF1A (“Tryp.-Res. eEF1A”) divided by total translated eEF1A (“eEF1A”).

Recombinant protein expression and purification

2xHA-Aim29: Expression vectors for 2xHA-Aim29 were cloned into a pET16b vector that was modified to have a 10xHis tag and 2xHA tag at the N-terminus. Rosetta (DE3) cells were transformed with the expression plasmids and grown at 37°C in LB media until reaching OD_{600} of 0.4-0.6. The cultures were then treated with 0.4 mM IPTG and shifted to 30°C to shake for 3 more hours. Cells were then collected by centrifugation at 5,000 x g for 15 minutes at 4°C. Cells were rinsed once in ice cold PBS and then pellets were snap frozen in liquid nitrogen and stored at −80°C until purification.

Cell pellets were thawed at 4°C and then resuspended in imidazole lysis buffer (20 mM Tris-HCl pH 7.5, 150 mM NaCl, 25 mM imidazole, 10 mM Beta-mercaptoethanol) supplemented with benzonase (10 U/mL) and 1x protease inhibitor cocktail (Roche). Cells were lysed with 4 passes on an Emulsiflex cell disruptor at ~12,000 - 15,000 PSI. Lysates were clarified by centrifugation at 20,000 x g for 10 minutes at 4°C. Clarified lysates were then passed over HisPur Ni-NTA resin that was equilibrated in 10 column volumes of lysis buffer (lacking benzonase or protease inhibitor cocktail). Clarified lysates were passed over the resin bed twice by gravity flow. The resin bed was then washed with 25 column volumes of lysis buffer and 25 column volumes of wash buffer (20 mM Tris-HCl pH 7.5, 150 mM NaCl, 75 mM imidazole, 10 mM Beta-mercaptoethanol). Bound proteins were eluted in 4 fractions of 1.5 column volumes each of elution buffer (20 mM Tris-HCl pH 7.5, 150 mM NaCl, 250 mM imidazole). The two fractions with the most target protein, as determined by SDS-PAGE and coomassie staining, were pooled and desalted into SEC buffer (50 mM Tris pH 7.5, 200 mM NaCl, 10% glycerol, 0.5 mM TCEP) using Econo-Pac 10DG Desalting columns (Bio-Rad). Samples were concentrated to ~1.5 mL using an Amicon ultra centrifugal concentrator with a 10 kDa cutoff. A volume of 1.5 mL of concentrated protein was then subjected to gel filtration on a Superdex 75 Increase 10/300 GL column equilibrated in SEC buffer. Peak fractions that ran near the expected molecular weight of a monomeric protein were analyzed via SDS-PAGE and coomassie staining, pooled, aliquoted, snap frozen in liquid nitrogen, and stored at −80°C.

Zpr1-3xFLAG: Zpr1-3xFLAG was recombinantly expressed and purified as previously described[6]. Zpr1-3xFLAG constructs were cloned into pET16b vectors with N-terminal 10xHis-3C tag and a 3xFLAG C-terminal tag. Rosetta (DE3) cells were transformed with

these vectors and grown at 37°C in Terrific Broth (TB) media until OD_{600} of 0.4. The cultures were then cooled down at 4°C for 1 hour and supplemented with 1 mM IPTG (US Biological Life Sciences) to induce protein expression at 16°C for 16 hours. Cells were harvested at 3,500 x g for 20 min and resuspended in PBS. After a second spin, cell pellets were frozen in liquid nitrogen and stored at −80 until purification.

Cell pellets were thawed at 4°C, resuspended in B1 Lysis Buffer (20 mM sodium phosphate pH 8.0, 300 mM NaCl, 20 mM imidazole) supplemented with benzonase (Millipore Sigma), 5 mM Beta-mercaptoethanol, Protease inhibitor cocktail and 0.2 mM PMSF. Cells were lysed with 5 passes on an Emulsiflex cell disruptor at ~12-15k PSI. Lysed cells were spun down at 28,000 x g for 30 min at 4°C in a JLA 16.25 rotor. Supernatant was loaded on an equilibrated 5 mL HisTrap HP column. The column was washed with 10 column volumes of B1 buffer before eluting with a linear gradient of B2 Elution Buffer (20mM sodium phosphate pH 8.0, 300 mM NaCl, 500 mM imidazole, 5 mM Beta-mercaptoethanol) over 5 column volumes. Peak elution fractions were pooled and concentrated to 2.5 mL with a 10 kDa cutoff filter before desalting with a PD10 desalting column into B3 Low-salt Anion Exchange Buffer (50 mM Tris pH 8.0, 50 mM NaCl, 5 mM Beta-mercaptoethanol). Desalted samples were applied to an equilibrated 5 mL HiTrap Q FF column, washed with 5 column volumes of B3 buffer, and eluted with a linear gradient of B4 High-salt Anion Exchange Buffer (50 mM Tris pH 8.0, 1 M NaCl, 5 mM Beta-mercaptoethanol) over 20 column volumes. Peak fractions were pooled and concentrated to <500 µL and applied to an equilibrated Superdex 200 10/300 column for gel filtration in B5 SEC buffer (50 mM Tris pH 8.0, 200 mM NaCl, 10% glycerol, 0.5 mM TCEP). Peak fractions were aliquoted, frozen in liquid nitrogen and stored at −80°C.

Lgt3 glucosyltransferase: Lgt3 from *Legionella pneumophila* was synthesized as an *E. coli* codon-optimized gBlock (Integrated DNA Technologies) and cloned into the BamHI/SalI site of a pET28a expression plasmid containing an N-terminal 6xHis tag. To facilitate gBlock synthesis we removed the short repetitive sequence encoding the “KXEEEQRI” repeat region [58]. Rosetta DE3 cells (Novagen) transformed with the expression plasmid were grown at 37°C in LB until reaching OD_{600} 0.4. Cells were then shifted to 30°C and IPTG was added to 0.4 mM to induce protein expression for 3 hours. Cells were collected via centrifugation at 5,000 x g for 15 minutes. Cell pellets were rinsed once in 25 mL ice cold PBS and then snap frozen in liquid nitrogen and stored at −80°C until lysis.

Cell pellets were thawed at 4°C and then resuspended in 25 mL lysis buffer (20 mM Tris-HCl pH 7.4, 150 mM NaCl, 25 mM imidazole) supplemented with 250 U benzonase nuclease (Millipore Sigma), 1x protease inhibitor cocktail (Roche), and 10 mM Beta-mercaptoethanol. Cells were lysed with 5 passes on an Emulsiflex cell disruptor at ~12-15k PSI. Lysates were spun down at 20,000 x g for 15 min at 4°C. Supernatant was loaded on an equilibrated 5 mL HisTrap HP column and washed with 20 column volumes of lysis buffer before being eluted on a linear gradient of elution buffer () over 5 column volumes. Peak fractions were concentrated on an Amicon 10 kDa cutoff centrifugal filter unit, aliquoted, snap frozen in liquid nitrogen, and stored at −80°C.

Purification of native eEF1A from yeast—Native eEF1A was purified from *S. cerevisiae* as previously described [6]. VDY465 (WT) cells were grown in large cultures to OD_{600} 1.8 in liquid YPD media. 3 L of cells were spun down at 3500 x g for 20 minutes at 4°C, washed in 50 mL ddH2O twice and resuspended in 1 mL per gram of pellet of resuspension buffer (1.2% PVP-40, 20 mM HEPES pH 7.4, 1x protease inhibitor cocktail [Roche], 1% solution P [2 mg Pepstatin A, 90 mg PMSF, 5 mL 100% ethanol], 1 mM DTT). Cells were spun down twice at 3500 x g for 10 minutes to remove all buffer. Cell paste was placed into a syringe and was pushed out to be frozen as "noodles" in a 50 mL conical tube filled with liquid nitrogen. Liquid nitrogen was decanted from the tube and frozen "noodles" were stored at −80°C until cryogenically lysed using a Retsch PM100 ball mill.

Next, 8 g of frozen grindate was thawed in 80 mL I-100 buffer (20 mM Tris pH 7.5, 0.1 mM EDTA, 100 mM KCl, 25% glycerol, 1 mM DTT) supplemented with 1x protease inhibitor cocktail (Roche). Lysate was spun at 8,000 x g for 5 min at 4°C in a JA 25.5 rotor. Supernatant was transferred into new tubes and spun at 20,000 x g for 15 min at 4°C in JA 25.5 rotor. Supernatant was then spun at 54,400 RPM for 106 min at 4°C in Ti 70 ultracentrifuge rotor. Supernatant was incubated with 10 g pre-equilibrated DEAE resin (in buffer I-100) for 1 hour while agitated on a tilt table at 4°C. Unbound fraction was removed by centrifugation. The resin was washed with an additional 20 mL I-100 buffer, spun down and the wash was added to the unbound fraction. The unbound fraction and wash was incubated with 60 mL pre-equilibrated CM-sepharose slurry (in buffer I-100) for 1 hour while agitated on a tilt table at 4°C. A buchner funnel with Whatman type 1 paper (~11 micron pore size) was used to separate the unbound fraction. The resin was washed with 40 mL I-100 before removing from the buchner funnel, resuspending in 60 mL I-100 with solid KCl supplemented to 500 mM final concentration of KCl, and incubating for 1 hour while agitated on a tilt table at 4°C. Eluate was collected using the buchner funnel, and resin was washed with an additional 20 mL buffer I-100 supplemented with solid KCl for a final concentration of 500 mM KCl, which was combined with the eluate. Eluate was concentrated with a 30 kDa cutoff concentrator to ~5 mL, filtered with a 0.22 micron filter and desalted into I-50 buffer (20 mM Tris pH 7.5, 0.1 mM EDTA, 50 mM KCl, 25% glycerol, 1 mM DTT) using 4 x 5 mL sequential HiTrap desalting columns. ~8 mL of flow-through was collected and applied onto a Source 15S 4.6/100 column. The column was washed with 40 CVs of I-50 buffer before eluting with a linear gradient of I-300 buffer (20 mM Tris pH 7.5, 0.1 mM EDTA, 300 mM KCl, 25% glycerol, 1 mM DTT) over 20 CVs. Peak fractions containing eEF1A were pooled and concentrated to ~2 mL with a 30 kDa cutoff concentrator. Sample was applied onto a HiPrep 16/60 Sephacryl S-100 column. Native eEF1A eluted as the second peak. Fractions were pooled and concentrated with a 30 kDa cutoff concentrator. Aliquots were frozen in liquid nitrogen and stored at −80°C.

GTPase assays

Enzyme-linked inorganic phosphate assay: The enzyme-linked inorganic phosphate assay was performed using the GTPase Kinetic ELIPA Assay Kit from Cytoskeleton, Inc. Reactions contained 100 nM eEF1A and 2 μM of Zpr1-3xFLAG variants as indicated in a total volume of 200 μL. Reactions were set up in 96-well plates in reaction buffer with low glycerol (20 mM Tris-HCl pH 7.5, 10 mM $Mg(OAc)_2$, 100 mM KCl,

1 mM DTT, 5% glycerol) and kit components according to manufacturer instructions. eEF1A was added before Zpr1-3xFLAG proteins or GTP and then incubated at room temperature for 10 minutes. Then, recombinant Zpr1-3xFLAG protein (Zpr1-3xFLAG^{WT} or Zpr1-3xFLAG^{ZnFMUT}) was added and incubated for 10 additional minutes at 30°C to allow complexes to form and reaction mixes to equilibrate to 30°C. GTP was added to 1 mM and mixed rapidly to initiate the reaction. Readings of absorbance at 360 nm were taken every 45 seconds using a SpectraMax i3 plate reader set to 30°C with continuous mixing. Reactions with Zpr1 and eEF1A were performed in duplicate and the average is plotted. Reactions with each protein alone to measure background GTPase activity were performed in one well. For the plot shown in Figure S3C the absorbance value at time 0 was set to 0 to account for small differences in starting absorbance between each well.

Hydrolysis of α-^{32}P-GTP: Reactions were set up at room temperature in reaction buffer (20 mM Tris-HCl pH 7.5, 10 mM $Mg(OAc)_2$, 100 mM KCl, 1 mM DTT, 5% glycerol) with eEF1A alone at the concentration indicated in each figure and allowed to incubate for 10 minutes at room temperature. Then, the indicated Zpr1-3xFLAG protein was added to the concentration indicated in each figure and incubated for 10 additional minutes at room temperature. The reactions were then placed on ice and a mixture of α-^{32}P-labeled GTP and unlabeled GTP was added to the reaction. The total concentration of labeled and unlabeled GTP varied across experiments and concentrations are indicated in figure legends. The reactions were mixed and placed in a 30°C thermal cycler to initiate the reaction. When included, the indicated 2xHA-Aim29 protein was added and mixed shortly before placing the tubes on ice. At each time point in the reaction an aliquot of 2 μL was removed and plunged into 8 μL of 50% formic acid to quench, vortexed, and placed on ice. 0.5-1 μL of each sample was analyzed by thin layer chromatography on PEI-cellulose plates (pre-run in water) using 0.5 M KH_2PO_4 as the solvent. Plates were run for 30 minutes, dried, and then analyzed via autoradiography and phosphor imaging.

ColabFold modeling of Zpr1•eEF1A•Aim29 complexes—ColabFold version 1.5.2 was used with 5 models, 100 seeds, 20 recycles and the default parameters with msa_mode: “MMseqs2 (UniRef+Environmental)”, and model_type: “AlphaFold2-multimer-v3” to model the *S. cerevisiae* Zpr1•eEF1A and Zpr1•eEF1A•Aim29 complexes. Sequences were obtained from Uniprot. Figure 3A/6A highlighted residues on eEF1A are: 36-75 (Switch I), 95-110 (Switch II), and 14-21 (P-loop). Zpr1 N-half (residues 1-280) was removed from models for clarity. Confidence scores for Figure 3B were calculated with the formula: (0.2*pTM + 0.8*ipTM) to get the “multimer” model confidence metric used for ranking models[9,59]. Predicted template-modeling score (pTM) assesses the overall accuracy of the model whereas interface predicted template-modeling score (ipTM) takes into account the interactions between residues of different proteins. GTP nucleotide was modeled into Figure 3A and Figure 6A using AlphaFill[30] with default parameters. Models are provided in Supplementary Item 1. Consurf[60] was used to determine conservation scores for Aim29 residues and CLUSTAL Omega[61] was used for sequence alignment as shown in Figure S2E. Molecular graphics and analyses for all models were performed with UCSF ChimeraX[62].

QUANTIFICATION AND STATISTICAL ANALYSIS

Differential gene-expression analysis of RNA sequencing data—Raw reads from Illumina HiSeq were checked for read quality using FastQC (v. 0.11.5) and aligned to the reference genome S288c (v. R64-3-1) using the RNA-seq aligner STAR (v.2.7.0). Gene read counts obtained from STAR were passed to the Bioconductor package DESeq2 (v. 1.34.0) to identify differentially expressed genes in VDY5662 and VDY5849 relative to VDY3334. Genes with Benjamini-Hochberg FDR < 0.05 were defined as significant.

RNA sequencing gene signature trend analysis—Raw read counts obtained post-alignment using STAR[63] for all samples were normalized and regularized-log (rlog) transformed using DESeq2[64]. Results of DESeq2 analysis are shown in Table S1. To identify if Hsf1 targets (28 targets obtained from Solis et al.) or Gcn4 targets (163 positively regulated targets obtained from SGD) clustered in a particular trend across samples, the clustering tool, degPatterns, from the DEGreport (v. 1.30.0) package was run on the normalized, regularized log transformed read counts filtered to include only the genes in the Hsf1 or Gcn4 target list.

Flow cytometry analysis—Samples were gated to retain live cells and discard doublets using BioConductor packages flowCore and flowViz. Each sample was normalized to cell size by dividing the raw YFP or GFP intensity (FITC.A) by side scatter (SSC.A). Data was log transformed for histograms and bar graphs and plotted using the R packages ggplot and ggridges.

Immunoblot and autoradiography quantification—Immunoblots and autoradiographs were quantified using the BandPeakQuantification ImageJ (FIJI) plugin (dx.doi.org/10.17504/protocols.io.7vghn3w).

Ribo-seq analysis—The four random nucleotides present in the RT primers used for library generation were trimmed from the 5’ end of reads with seqtk (https://github.com/lh3/seqtk) using options “trimfq -b 4”. Next, 3’ adapter sequences were removed using cutadapt (https://cutadapt.readthedocs.io/en/stable/index.html). Trimmed fastq files were then collapsed to fasta files and subsequently aligned and analyzed using RiboToolkit [65] to obtain ribosome footprint length distributions. To normalize samples by sequencing depth and compare fold change in ribosome occupancy, sorted bam files obtained from RiboToolkit were run through bamCompare from the deepTools suite. The resulting bigWig file was visualized in IGV.

Supplementary Material

Refer to Web version on PubMed Central for supplementary material.

Acknowledgements

We thank Andrew Kane and Jeffrey Prince for their efforts during the project’s inception; Jack Taunton, Scott Blanchard, and William Merrick for discussions about eEF1A’s structure and enzymology; Onn Brandman for the Gcn4 reporter plasmid; Swapnil Parhad and Danesh Moazed for *S. pombe* vectors, strains, and additional advice; Dan Spatt and Fred Winston for *S. pombe* vectors; Tom Jones for his insight into Aim29’s evolutionary origins.

V.D. personally thanks Charlie Hoffman for *S. pombe* cDNA libraries and advice. This work was supported by the National Institutes of Health (R35-GM127136 to V.D.) and the National Science Foundation Graduate Research Fellowships Program (DGE1745303 to A.J.M. and I.M.S).

References

1. Balchin D, Hayer-Hartl M, and Hartl FU (2016). In vivo aspects of protein folding and quality control. Science 353, aac4354. 10.1126/science.aac4354. [PubMed: 27365453]
2. Solís EJ, Pandey JP, Zheng X, Jin DX, Gupta PB, Airoldi EM, Pincus D, and Denic V (2016). Defining the Essential Function of Yeast Hsf1 Reveals a Compact Transcriptional Program for Maintaining Eukaryotic Proteostasis. Mol. Cell 63, 60–71. 10.1016/j.molcel.2016.05.014. [PubMed: 27320198]
3. Rosenzweig R, Nillegoda NB, Mayer MP, and Bukau B (2019). The Hsp70 chaperone network. Nat. Rev. Mol. Cell Biol 20, 665–680. 10.1038/s41580-019-0133-3. [PubMed: 31253954]
4. Schopf FH, Biebl MM, and Buchner J (2017). The HSP90 chaperone machinery. Nat. Rev. Mol. Cell Biol 18, 345–360. 10.1038/nrm.2017.20. [PubMed: 28429788]
5. Pincus D, Anandhakumar J, Thiru P, Guertin MJ, Erkine AM, and Gross DS (2018). Genetic and epigenetic determinants establish a continuum of Hsf1 occupancy and activity across the yeast genome. Mol. Biol. Cell 29, 3168–3182. 10.1091/mbc.E18-06-0353. [PubMed: 30332327]
6. Sabbarini IM, Reif D, McQuown AJ, Nelliat AR, Prince J, Membreno BS, Wu CC-C, Murray AW, and Denic V (2023). Zinc-finger protein Zpr1 is a bespoke chaperone essential for eEF1A biogenesis. Mol. Cell 83, 252–265.e13. 10.1016/j.molcel.2022.12.012. [PubMed: 36630955]
7. Maruyama K, Imai H, Kawamura M, Ishino S, Ishino Y, Ito K, and Uchiumi T (2019). Switch of the interactions between the ribosomal stalk and EF1A in the GTP- and GDP-bound conformations. Sci. Rep 9, 14761. 10.1038/s41598-019-51266-x. [PubMed: 31611569]
8. Polekhina G, Thirup S, Kjeldgaard M, Nissen P, Lippmann C, and Nyborg J (1996). Helix unwinding in the effector region of elongation factor EF-Tu–GDP. Structure 4, 1141–1151. 10.1016/S0969-2126(96)00122-0. [PubMed: 8939739]
9. Mirdita M, Schütze K, Moriwaki Y, Heo L, Ovchinnikov S, and Steinegger M (2022). ColabFold: making protein folding accessible to all. Nat. Methods 19, 679–682. 10.1038/S41592-022-01488-1. [PubMed: 35637307]
10. Reinle K, Mogk A, and Bukau B (2022). The Diverse Functions of Small Heat Shock Proteins in the Proteostasis Network. J. Mol. Biol 434, 167157. 10.1016/j.jmb.2021.167157. [PubMed: 34271010]
11. Koldewey P, Stull F, Horowitz S, Martin R, and Bardwell JCA (2016). Forces Driving Chaperone Action. Cell 166, 369–379. 10.1016/j.cell.2016.05.054. [PubMed: 27293188]
12. Stull F, Koldewey P, Humes JR, Radford SE, and Bardwell JCA (2016). Substrate protein folds while it is bound to the ATP-independent chaperone Spy. Nat. Struct. Mol. Biol 23, 53–58. 10.1038/nsmb.3133. [PubMed: 26619265]
13. Papasergi-Scott MM, Kwarcinski F, Yu M, Panova O, Ovrutsky AM, Skiniotis G, and Tall G (2022). Structures of Ric-8B in Complex With Gα Protein Folding Clients Reveal Isoform Specificity Mechanisms. SSRN Electron. J 10.2139/ssrn.4254228.
14. Seven AB, Hilger D, Papasergi-Scott MM, Zhang L, Qu Q, Kobilka BK, Tall GG, and Skiniotis G (2020). Structures of Gα Proteins in Complex with Their Chaperone Reveal Quality Control Mechanisms. Cell Rep. 30, 3699–3709.e6. 10.1016/j.celrep.2020.02.086. [PubMed: 32126208]
15. Tall GG, Krumins AM, and Gilman AG (2003). Mammalian Ric-8A (Synembryn) Is a Heterotrimeric Gα Protein Guanine Nucleotide Exchange Factor. J. Biol. Chem 278, 8356–8362. 10.1074/jbc.M211862200. [PubMed: 12509430]
16. Tall GG, and Gilman AG (2004). Purification and Functional Analysis of Ric-8A: A Guanine Nucleotide Exchange Factor for G-Protein α Subunits. In Methods in Enzymology (Elsevier), pp. 377–388. 10.1016/S0076-6879(04)90023-7.
17. Usaj M, Tan Y, Wang W, VanderSluis B, Zou A, Myers CL, Costanzo M, Andrews B, and Boone C (2017). TheCellMap.org: A Web-Accessible Database for Visualizing and Mining the Global Yeast Genetic Interaction Network. G3 GenesGenomesGenetics 7, 1539–1549. 10.1534/g3.117.040220.

18. Mistry J, Chuguransky S, Williams L, Qureshi M, Salazar GA, Sonnhammer ELL, Tosatto SCE, Paladin L, Raj S, Richardson LJ, et al. (2021). Pfam: The protein families database in 2021. Nucleic Acids Res. 49, D412–D419. 10.1093/nar/gkaa913. [PubMed: 33125078]
19. Geiler-Samerotte KA, Dion MF, Budnik BA, Wang SM, Hartl DL, and Drummond DA (2011). Misfolded proteins impose a dosage-dependent fitness cost and trigger a cytosolic unfolded protein response in yeast. Proc. Natl. Acad. Sci 108, 680–685. 10.1073/pnas.1017570108. [PubMed: 21187411]
20. Pincus D. (2020). Regulation of Hsf1 and the Heat Shock Response. Adv. Exp. Med. Biol 1243, 41–50. 10.1007/978-3-030-40204-4_3. [PubMed: 32297210]
21. Nieto-Sotelo J, Wiederrecht G, Okuda A, and Parker CS (1990). The yeast heat shock transcription factor contains a transcriptional activation domain whose activity is repressed under nonshock conditions. Cell 62, 807–817. 10.1016/0092-8674(90)90124-W. [PubMed: 2201453]
22. Sorger PK (1990). Yeast heat shock factor contains separable transient and sustained response transcriptional activators. Cell 62, 793–805. 10.1016/0092-8674(90)90123-V. [PubMed: 2201452]
23. Zheng X, Krakowiak J, Patel N, Beyzavi A, Ezike J, Khalil AS, and Pincus D (2016). Dynamic control of Hsf1 during heat shock by a chaperone switch and phosphorylation. eLife 5, e18638. 10.7554/eLife.18638. [PubMed: 27831465]
24. Hinnebusch AG (2005). TRANSLATIONAL REGULATION OF *GCN4* AND THE GENERAL AMINO ACID CONTROL OF YEAST. Annu. Rev. Microbiol 59, 407–450. 10.1146/annurev.micro.59.031805.133833. [PubMed: 16153175]
25. Wu CC-C, Zinshteyn B, Wehner KA, and Green R (2019). High-Resolution Ribosome Profiling Defines Discrete Ribosome Elongation States and Translational Regulation during Cellular Stress. Mol. Cell 73, 959–970.e5. 10.1016/j.molcel.2018.12.009. [PubMed: 30686592]
26. Belyi Y, Stahl M, Sovkova I, Kaden P, Luy B, and Aktories K (2009). Region of Elongation Factor 1A1 Involved in Substrate Recognition by Legionella pneumophila Glucosyltransferase Lgt1. J. Biol. Chem 284, 20167–20174. 10.1074/jbc.M109.008441. [PubMed: 19478083]
27. Tzivelekidis T, Jank T, Pohl C, Schlosser A, Rospert S, Knudsen CR, Rodnina MV, Belyi Y, and Aktories K (2011). Aminoacyl-tRNA-charged eukaryotic elongation factor 1A is the bona fide substrate for Legionella pneumophila effector glucosyltransferases. PloS One 6, e29525. 10.1371/journal.pone.0029525. [PubMed: 22216304]
28. Wang M, Herrmann CJ, Simonovic M, Szklarczyk D, and Mering C (2015). Version 4.0 of PaxDb: Protein abundance data, integrated across model organisms, tissues, and cell-lines. PROTEOMICS 15, 3163–3168. 10.1002/pmic.201400441. [PubMed: 25656970]
29. Humphreys IR, Pei J, Baek M, Krishnakumar A, Anishchenko I, Ovchinnikov S, Zhang J, Ness TJ, Banjade S, Bagde SR, et al. (2021). Computed structures of core eukaryotic protein complexes. Science 374, eabm4805. 10.1126/science.abm4805. [PubMed: 34762488]
30. Hekkelman ML, de Vries I, Joosten RP, and Perrakis A (2023). AlphaFill: enriching AlphaFold models with ligands and cofactors. Nat. Methods 20, 205–213. 10.1038/S41592-022-01685-y. [PubMed: 36424442]
31. Cavallius J, and Merrick WC (1998). Site-directed Mutagenesis of Yeast eEF1A. J. Biol. Chem 273, 28752–28758. 10.1074/jbc.273.44.28752. [PubMed: 9786872]
32. Holm M, Natchiar SK, Rundlet EJ, Myasnikov AG, Watson ZL, Altman RB, Wang H-Y, Taunton J, and Blanchard SC (2023). mRNA decoding in human is kinetically and structurally distinct from bacteria. Nature. 10.1038/s41586-023-05908-w.
33. Shao S, Murray J, Brown A, Taunton J, Ramakrishnan V, and Hegde RS (2016). Decoding Mammalian Ribosome-mRNA States by Translational GTPase Complexes. Cell 167, 1229–1240.e15. 10.1016/j.cell.2016.10.046. [PubMed: 27863242]
34. Daviter T, Wieden H-J, and Rodnina MV (2003). Essential Role of Histidine 84 in Elongation Factor Tu for the Chemical Step of GTP Hydrolysis on the Ribosome. J. Mol. Biol 332, 689–699. 10.1016/S0022-2836(03)00947-1. [PubMed: 12963376]
35. Brandman O, Stewart-Ornstein J, Wong D, Larson A, Williams CC, Li G-W, Zhou S, King D, Shen PS, Weibezahn J, et al. (2012). A Ribosome-Bound Quality Control Complex Triggers Degradation of Nascent Peptides and Signals Translation Stress. Cell 151, 1042–1054. 10.1016/j.cell.2012.10.044. [PubMed: 23178123]

36. Chinali G, Wolf H, and Parmeggiani A (1977). Effect of Kirromycin on Elongation Factor Tu. Location of the Catalytic Center for Ribosome . Elongation-Factor-Tu GTPase Activity on the Elongation Factor. Eur. J. Biochem 75, 55–65. 10.1111/j.1432-1033.1977.tb11503.x. [PubMed: 193689]
37. Fasano O, Bruns W, Crechet J-B, Sander G, and Parmeggiani A (1978). Modification of Elongation-Factor-Tu . Guanine-Nucleotide Interaction by Kirromycin. A Comparison with the Effect of Aminoacyl-tRNA and Elongation Factor Ts. Eur. J. Biochem 89, 557–565. 10.1111/j.1432-1033.1978.tb12560.x. [PubMed: 251130]
38. Wolf H, Chinali G, and Parmeggiani A (1974). Kirromycin, an Inhibitor of Protein Biosynthesis that Acts on Elongation Factor Tu. Proc. Natl. Acad. Sci 71, 4910–4914. 10.1073/pnas.71.12.4910. [PubMed: 4373734]
39. Vogeley L, Palm GJ, Mesters JR, and Hilgenfeld R (2001). Conformational Change of Elongation Factor Tu (EF-Tu) Induced by Antibiotic Binding. J. Biol. Chem 276, 17149–17155. 10.1074/jbc.M100017200. [PubMed: 11278992]
40. Kobayashi K, Saito K, Ishitani R, Ito K, and Nureki O (2012). Structural basis for translation termination by archaeal RF1 and GTP-bound EF1α complex. Nucleic Acids Res. 40, 9319–9328. 10.1093/nar/gks660. [PubMed: 22772989]
41. Voorhees RM, Schmeing TM, Kelley AC, and Ramakrishnan V (2010). The Mechanism for Activation of GTP Hydrolysis on the Ribosome. Science 330, 835–838. 10.1126/science.1194460. [PubMed: 21051640]
42. Mishra AK, Gangwani L, Davis RJ, and Lambright DG (2007). Structural insights into the interaction of the evolutionarily conserved ZPR1 domain tandem with eukaryotic EF1A, receptors, and SMN complexes. Proc. Natl. Acad. Sci 104, 13930–13935. 10.1073/pnas.0704915104. [PubMed: 17704259]
43. Nithianantham S, Le S, Seto E, Jia W, Leary J, Corbett KD, Moore JK, and Al-Bassam J (2015). Tubulin cofactors and Arl2 are cage-like chaperones that regulate the soluble αβ-tubulin pool for microtubule dynamics. eLife 4, e08811. 10.7554/eLife.08811. [PubMed: 26208336]
44. Mönkemeyer L, Klaips CL, Balchin D, Körner R, Hartl FU, and Bracher A (2019). Chaperone Function of Hgh1 in the Biogenesis of Eukaryotic Elongation Factor 2. Mol. Cell 74, 88–100.e9. 10.1016/j.molcel.2019.01.034. [PubMed: 30876804]
45. Schopf FH, Huber EM, Dodt C, Lopez A, Biebl MM, Rutz DA, Mühlhofer M, Richter G, Madl T, Sattler M, et al. (2019). The Co-chaperone Cns1 and the Recruiter Protein Hgh1 Link Hsp90 to Translation Elongation via Chaperoning Elongation Factor 2. Mol. Cell 74, 73–87.e8. 10.1016/j.molcel.2019.02.011. [PubMed: 30876805]
46. Perzlmaier AF, Richter F, and Seufert W (2013). Translation Initiation Requires Cell Division Cycle 123 (Cdc123) to Facilitate Biogenesis of the Eukaryotic Initiation Factor 2 (eIF2). J. Biol. Chem 288, 21537–21546. 10.1074/jbc.M113.472290. [PubMed: 23775072]
47. Vanselow S, Neumann-Arnold L, Wojciech-Moock F, and Seufert W (2022). Stepwise assembly of the eukaryotic translation initiation factor 2 complex. J. Biol. Chem 298, 101583. 10.1016/j.jbc.2022.101583. [PubMed: 35031321]
48. Biebl MM, Lopez A, Rehn A, Freiburger L, Lawatscheck J, Blank B, Sattler M, and Buchner J (2021). Structural elements in the flexible tail of the co-chaperone p23 coordinate client binding and progression of the Hsp90 chaperone cycle. Nat. Commun 12, 828. 10.1038/s41467-021-21063-0. [PubMed: 33547294]
49. Biebl MM, and Buchner J (2023). p23 and Aha1: Distinct Functions Promote Client Maturation. In The Networking of Chaperones by Co-Chaperones Subcellular Biochemistry., Edkins AL and Blatch GL, eds. (Springer International Publishing), pp. 159–187. 10.1007/978-3-031-14740-1_6.
50. Biebl MM, Riedl M, and Buchner J (2020). Hsp90 Co-chaperones Form Plastic Genetic Networks Adapted to Client Maturation. Cell Rep. 32, 108063. 10.1016/j.celrep.2020.108063. [PubMed: 32846121]
51. Longtine MS, Mckenzie A III, Demarini DJ, Shah NG, Wach A, Brachat A, Philippsen P, and Pringle JR (1998). Additional modules for versatile and economical PCR-based gene deletion and modification in Saccharomyces cerevisiae. Yeast 14, 953–961. 10.1002/(SICI)1097-0061(199807)14:10<953::AID-YEA293>3.0.CO;2-U. [PubMed: 9717241]

52. Gietz RD, and Schiestl RH (2007). High-efficiency yeast transformation using the LiAc/SS carrier DNA/PEG method. Nat. Protoc 2, 31–34. 10.1038/nprot.2007.13. [PubMed: 17401334]
53. Brachmann CB, Davies A, Cost GJ, Caputo E, Li J, Hieter P, and Boeke JD (1998). Designer deletion strains derived fromSaccharomyces cerevisiae S288C: A useful set of strains and plasmids for PCR-mediated gene disruption and other applications. Yeast 14, 115–132. 10.1002/(SICI)1097-0061(19980130)14:2<115::AID-YEA204>3.0.CO;2-2. [PubMed: 9483801]
54. Shafieinouri M, Membreno BS, and Wu CC-C (2022). High-Resolution Ribosome Profiling for Determining Ribosome Functional States During Translation Elongation. In The Integrated Stress Response Methods in Molecular Biology., Matějů D and Chao JA, eds. (Springer US), pp. 173–186. 10.1007/978-1-0716-1975-9_11.
55. Janoo RTK, Neely LA, Braun BR, Whitehall SK, and Hoffman CS (2001). Transcriptional Regulators of the *Schizosaccharomyces pombe fbp1* Gene Include Two Redundant Tup1p-like Corepressors and the CCAAT Binding Factor Activation Complex. Genetics 157, 1205–1215. 10.1093/genetics/157.3.1205. [PubMed: 11238405]
56. Koschwanez JH, Foster KR, and Murray AW (2013). Improved use of a public good selects for the evolution of undifferentiated multicellularity. eLife 2, e00367. 10.7554/eLife.00367. [PubMed: 23577233]
57. Schuldiner M, Metz J, Schmid V, Denic V, Rakwalska M, Schmitt HD, Schwappach B, and Weissman JS (2008). The GET Complex Mediates Insertion of Tail-Anchored Proteins into the ER Membrane. Cell 134, 634–645. 10.1016/j.cell.2008.06.025. [PubMed: 18724936]
58. Belyi Y, Tabakova I, Stahl M, and Aktories K (2008). Lgt: a Family of Cytotoxic Glucosyltransferases Produced by *Legionella pneumophila*. J. Bacteriol 190, 3026–3035. 10.1128/JB.01798-07. [PubMed: 18281405]
59. Evans R, O'Neill M, Pritzel A, Antropova N, Senior A, Green T, Žídek A, Bates R, Blackwell S, Yim J, et al. (2021). Protein complex prediction with AlphaFold-Multimer (Bioinformatics) 10.1101/2021.10.04.463034.
60. Ashkenazy H, Abadi S, Martz E, Chay O, Mayrose I, Pupko T, and Ben-Tal N (2016). ConSurf 2016: an improved methodology to estimate and visualize evolutionary conservation in macromolecules. Nucleic Acids Res. 44, W344–W350. 10.1093/nar/gkw408. [PubMed: 27166375]
61. Madeira F, Pearce M, Tivey ARN, Basutkar P, Lee J, Edbali O, Madhusoodanan N, Kolesnikov A, and Lopez R (2022). Search and sequence analysis tools services from EMBL-EBI in 2022. Nucleic Acids Res. 50, W276–W279. 10.1093/nar/gkac240. [PubMed: 35412617]
62. Pettersen EF, Goddard TD, Huang CC, Meng EC, Couch GS, Croll TI, Morris JH, and Ferrin TE (2021). UCSF ChimeraX : Structure visualization for researchers, educators, and developers. Protein Sci. 30, 70–82. 10.1002/pro.3943. [PubMed: 32881101]
63. Dobin A, Davis CA, Schlesinger F, Drenkow J, Zaleski C, Jha S, Batut P, Chaisson M, and Gingeras TR (2013). STAR: ultrafast universal RNA-seq aligner. Bioinformatics 29, 15–21. 10.1093/bioinformatics/bts635. [PubMed: 23104886]
64. Love MI, Huber W, and Anders S (2014). Moderated estimation of fold change and dispersion for RNA-seq data with DESeq2. Genome Biol. 15, 550. 10.1186/s13059-014-0550-8. [PubMed: 25516281]
65. Liu Q, Shvarts T, Sliz P, and Gregory RI (2020). RiboToolkit: an integrated platform for analysis and annotation of ribosome profiling data to decode mRNA translation at codon resolution. Nucleic Acids Res. 48, W218–W229. 10.1093/nar/gkaa395. [PubMed: 32427338]

Highlights:

1. *aim29*Δ cells have eEF1A biogenesis defects suppressible by excess Zpr1
2. Zpr1-mediated folding of eEF1A requires client GTP hydrolysis
3. Aim29 senses the Zpr1•eEF1A folding complex in its GTP-bound state
4. Aim29 dampens folding complex GTPase activity to drive client release from Zpr1

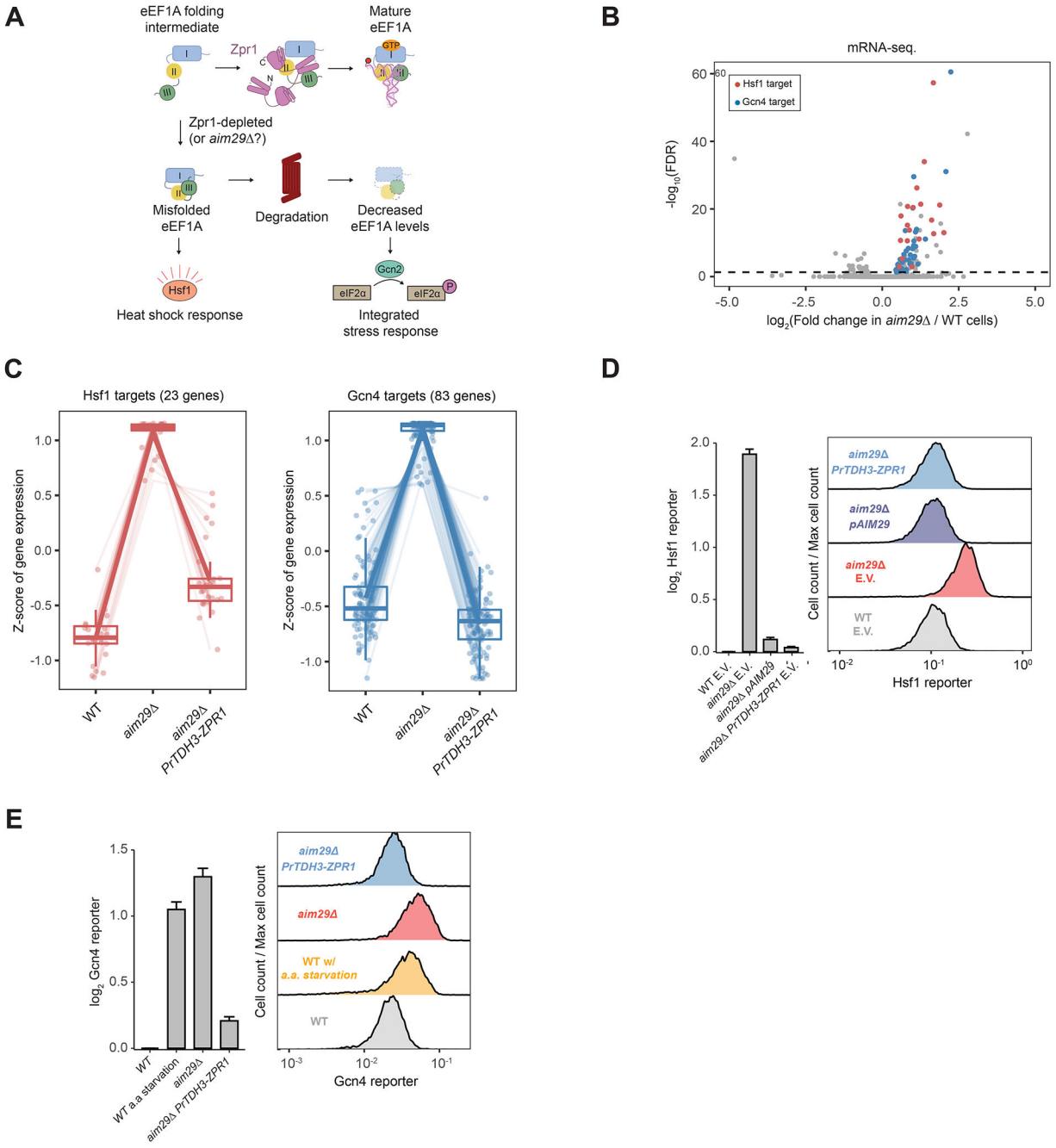

Figure 1. Coincident induction of Hsf1 and Gcn4 stress responses in cells lacking Aim29. See also Figure S1 and Supplemental Table 1.

(A) Cartoon schematic illustrating Zpr1's role in eEF1A biogenesis. In the absence of Zpr1, eEF1A misfolding activates Hsf1 and decreased levels of eEF1A lead to ISR activation and decreased translation[6]. (B) Wild-type (WT) and *aim29*Δ cells were analyzed by mRNA-sequencing. Volcano plot shows differentially expressed genes (FDR < 0.05, dashed line) with significantly upregulated genes in *aim29*Δ cells annotated as Hsf1 or Gcn4 targets. The 29% of differentially upregulated genes not annotated were found using GO enrichment analysis to be enriched for amino acid/amino acid precursor biosynthesis genes. See

Supplemental Table 1 for further details. (C) Indicated strains were subjected to mRNA sequencing. Each point denotes a gene in the indicated category, where the gene expression *Z*-score is obtained by gene-wise mean centering and scaling to the standard deviation across all samples. (D) Indicated strains carrying the Hsf1 reporter (4xHSE-YFP) were analyzed by flow cytometry. Bar graphs show median YFP intensity values normalized to cell size (side scatter area) and the average median YFP intensity of wild-type (WT) cells. Error bars represent standard deviation from three biological replicates. Representative histograms of median YFP intensity normalized to side scatter are shown. (E) Indicated strains carrying a Gcn4 reporter (Gcn4 upstream ORFs driving GFP expression) were analyzed by flow cytometry. The wild-type (WT) was subjected to one hour of amino acid starvation as a positive control. Bar graphs and histograms showing reporter activity were generated as in panel D.

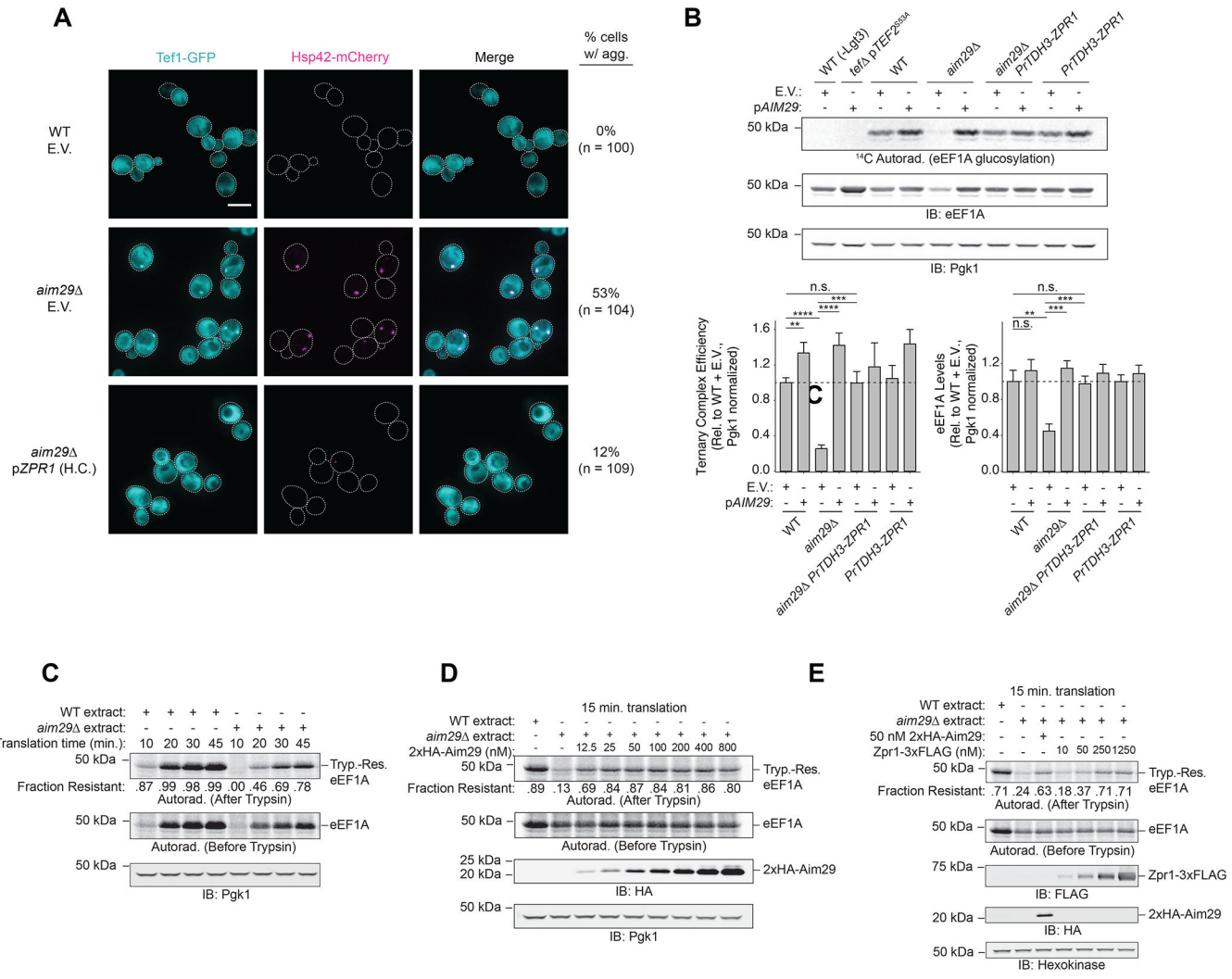

Figure 2. Aim29 is an eEF1A biogenesis factor.

(A) Strains with the indicated genotypes and expressing endogenously-tagged Tef1-GFP and Hsp42-mCherry were imaged by confocal microscopy. Shown are representative micrographs normalized to the same intensity, with cells outlined. The percentage of n cells with aggregates is indicated. (B) Native extracts from strains carrying either the empty vector (E.V.) or one expressing Aim29 under its endogenous promoter (p*AIM29*) were incubated with Lgt3 glucosyltransferase and UDP-^{14}C-glucose, followed by SDS-PAGE and immunoblotting or autoradiography. The "WT (-Lgt3)" reaction was performed on WT (w/ E.V). extracts. To assess glucosylation specificity, we analyzed *tef*Δ cells carrying a plasmid expressing *TEF2*^{S53A} from its endogenous promoter (p*TEF2*^{S53A}). Bar plots represent mean ± standard deviation of three replicates. Ternary complex efficiency is defined as ^{14}C autoradiography signal divided by eEF1A immunoblot signal normalized to Pgk1 immunoblot signal. An unpaired, one-sided, two-sample t test was used to compare conditions. ** $p < 0.01$; *** $p < 0.001$; **** $p < 0.0001$ (C) Resistance of ^{35}S-methionine-radiolabeled eEF1A to trypsin digestion was determined after initiating *in vitro* translation for the indicated times in wild type (WT) or *aim29*Δ extracts. Following digestion, samples

were resolved by SDS-PAGE and visualized by autoradiography or immunoblotting (IB). “Fraction resistant” is the signal of trypsin-resistant (Tryp.-Res.) eEF1A fragment divided by total synthesized eEF1A in the “Before Trypsin” panel. (D) As in panel C but with all reactions analyzed after 15 minutes of translation and with addition of 2xHA-Aim29 protein. (E) As in panel D, but with addition of 2xHA-Aim29 or Zpr1-3xFLAG protein.

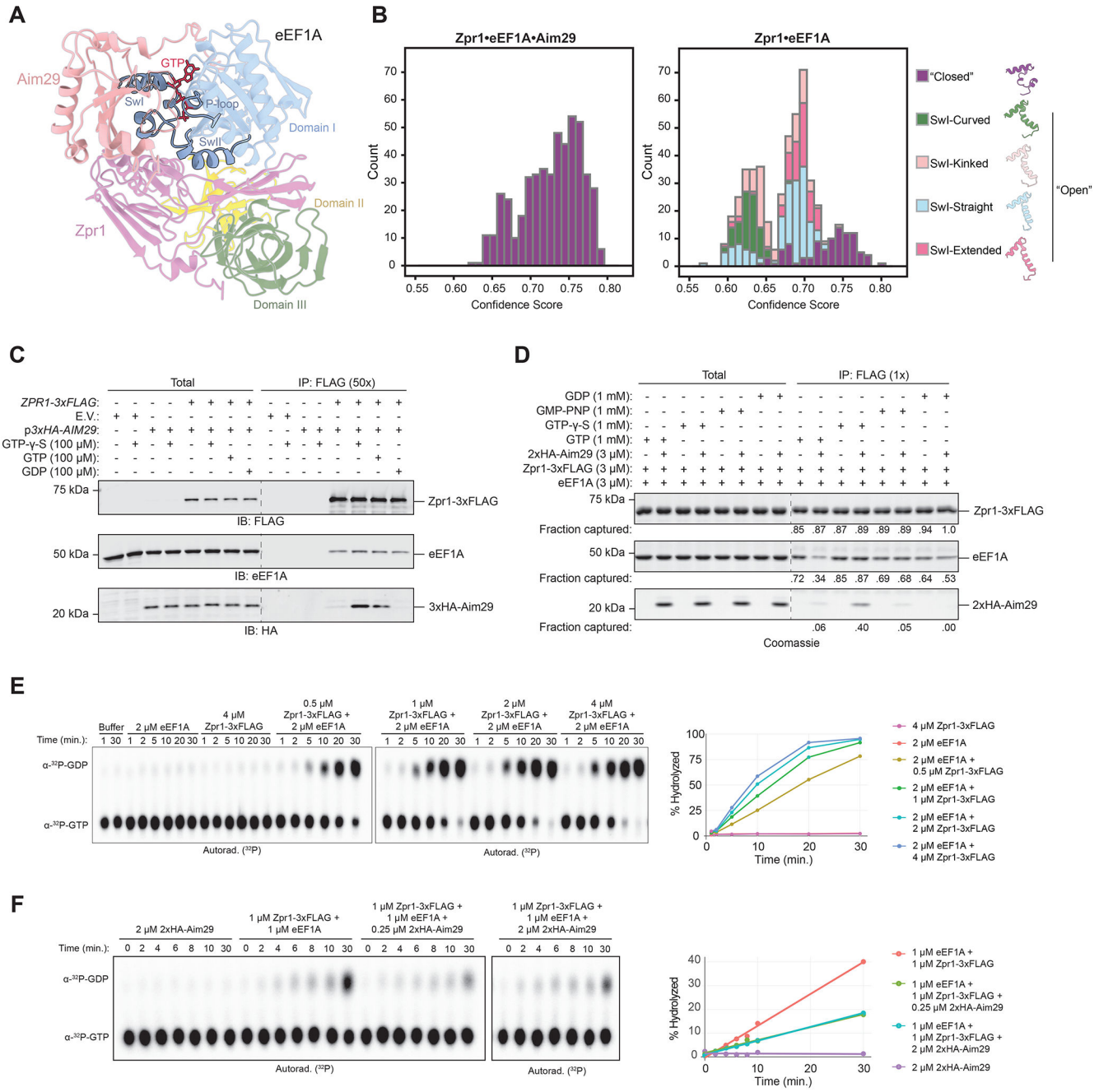

Figure 3. Aim29 is a conformational sensor of Zpr1•eEF1A in its GTP-bound, pre-hydrolysis state. See also Figures S2 and S3.

(A) Ribbon diagram of ColabFold model showing eEF1A (colored by domain) bound to Aim29 (salmon) and the C-terminal half of Zpr1 (purple). The N-terminal half of Zpr1 is removed for clarity. Switch I, Switch II, and P-loop regions of eEF1A are outlined in black. GTP (red) was modeled into the nucleotide pocket using AlphaFill. (B) Stacked histograms showing distribution of Switch I conformations in 500 ColabFold models for Zpr1•eEF1A•Aim29 or Zpr1•eEF1A binned by confidence score. (C) FLAG immunoprecipitation (IP) analysis of cell lysates, supplemented with nucleotides as

indicated, derived from *aim29*Δ cells with endogenous *ZPR1* locus untagged or expressing *ZPR1-3xFLAG* (−/+), and additionally carrying empty vector or a vector expressing 3xHA-Aim29 (−/+). Starting material (Total) and eluted (IP) fractions were analyzed by SDS-PAGE and immunoblotting. Dashes indicate cropping from the same immunoblot to remove irrelevant lanes. (D) FLAG IP of the indicated pure proteins prepared as described in STAR Methods. Total and eluted (IP) fractions were analyzed by SDS-PAGE and Coomassie staining. "Fraction captured" is the signal of IP over the corresponding total. Zpr1-3xFLAG was quantitatively captured under these conditions. Dashes indicate cropping from the same gel to remove irrelevant lanes. (E) Analysis of GTPase activity in the indicated protein samples. Reactions contained 100 μM unlabeled GTP and 100 nM α-^{32}P-GTP. Quenched reactions were analyzed by thin layer chromatography and autoradiography. Line plots show quantification of the representative autoradiograph shown. (F) As in panel E but with 200 μM unlabeled GTP, 100 nM α-^{32}P-GTP, and 2xHA-Aim29 where indicated.

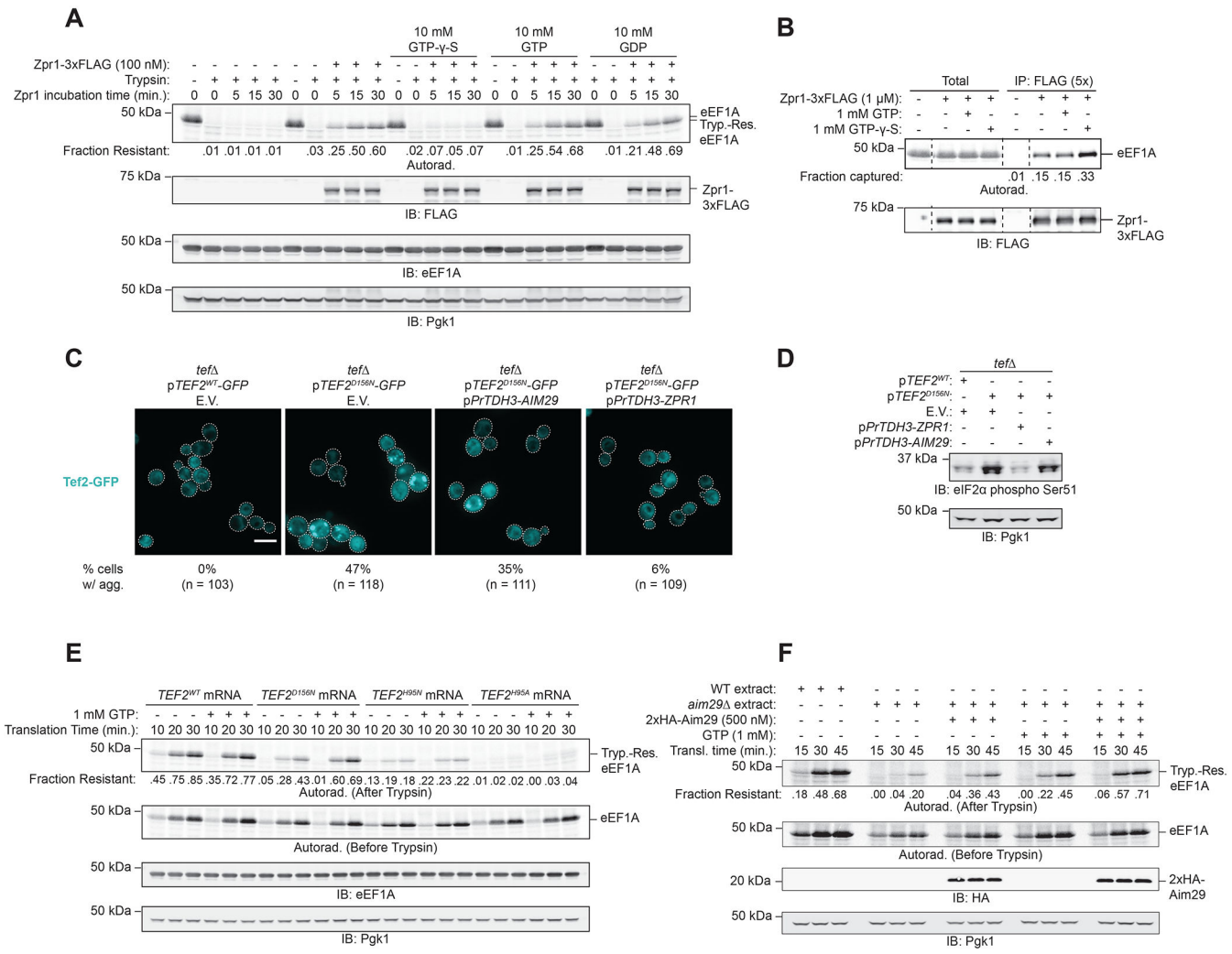

Figure 4. GTP binding and hydrolysis facilitate eEF1A biogenesis. See also Figures S3 and S4.

(A) Following *in vitro* translation of ^{35}S-methionine labeled eEF1A in Zpr1-depleted (*ZPR1-AID*) extracts, further synthesis was stopped with cycloheximide. Nucleotides were added where indicated, followed by Zpr1-3xFLAG. Aliquots removed after incubation with Zpr1-3xFLAG for the indicated times were analyzed by trypsin digestion as in Figure 2C. (B) FLAG IP analysis of samples prepared as in panel A. IP was initiated after 5 minutes of Zpr1-3xFLAG incubation time. Shown below is the fraction of eEF1A captured by quantitative IP of Zpr1-3xFLAG. Dashes indicate cropping from the same immunoblot or autoradiograph to remove irrelevant lanes. (C) Indicated *tef*Δ strains carrying the indicated *TEF2-GFP* plasmid and additionally carrying an empty vector (E.V.) or one overexpressing Aim29 and Zpr1 from the strong *TDH3* promoter were analyzed by confocal microscopy as in Figure 2A. (D) Whole cell lysates from the indicated strains were analyzed by SDS-PAGE and immunoblotting (IB) for eIF2α phospho-Ser51 and Pgk1. (E) Translation of the indicated ^{35}S-methionine-radiolabeled eEF1A variant was initiated in cell-free translation extracts and resistance to trypsin was determined at the indicated times. Additional GTP was added before translation where indicated. “Fraction resistant” is defined as in Figure 2C.

(F) As in panel E, but with eEF1A^{D156N} synthesized in wild type or *aim29*Δ extracts with recombinant 2xHA-Aim29 protein and/or 1 mM GTP added where indicated.

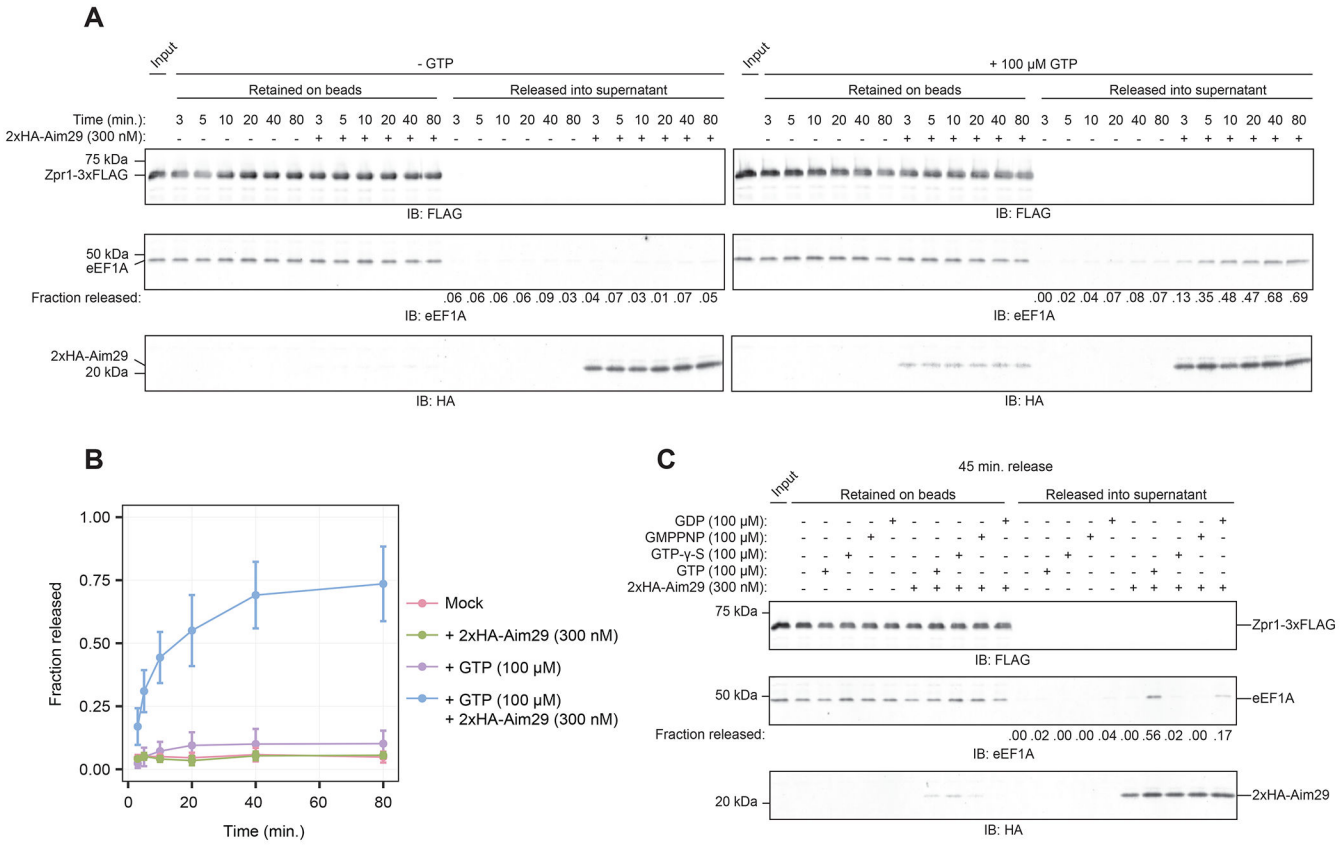

Figure 5. Aim29 requires GTP hydrolysis to destabilize the Zpr1•eEF1A complex. See also Figure S5.

(A) Zpr1-3xFLAG•eEF1A complexes were first immobilized on beads (~300 nM Zpr1 and ~150 nM eEF1A), which were subsequently incubated with or without 300 nM 2xHA-Aim29 and/or 100 μM GTP (left vs right panels). At different times samples were subjected to magnetic separation and removal of the supernatant fraction, followed by elution of the beads with FLAG peptide. Samples were resolved by SDS-PAGE and visualized by immunoblotting (IB). The “Input” lane represents beads that were directly eluted with FLAG peptide after the initial immobilization of Zpr1-3xFLAG•eEF1A. “Fraction released” is the eEF1A signal in each supernatant over the input signal. (B) Line plot showing quantification of eEF1A released from Zpr1-3xFLAG beads over time in panel A. Data represents mean ± standard deviation of four replicates. (C) As in panel A but with reactions analyzed at 45 minutes of incubation time with 2xHA-Aim29 and/or the indicated nucleotides.

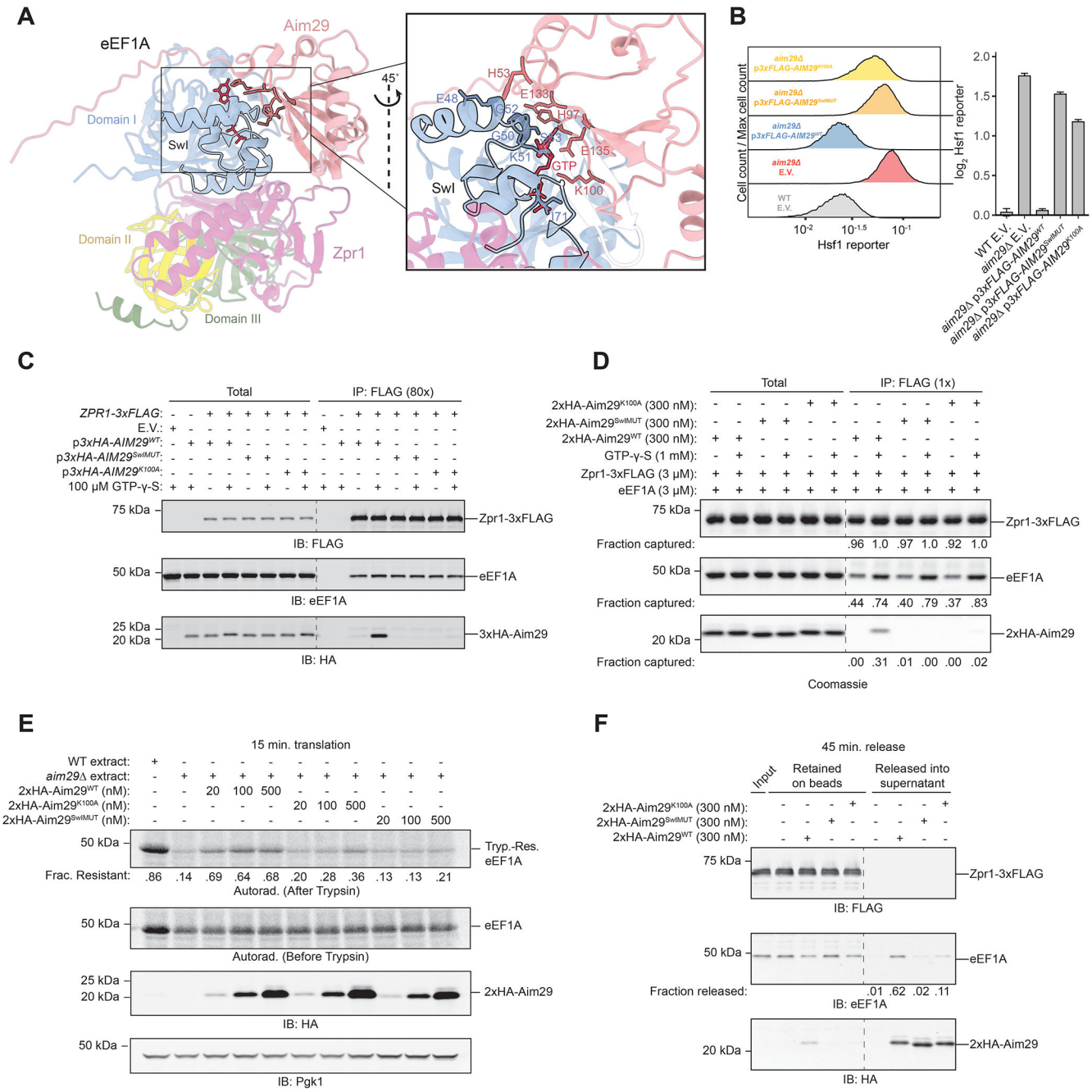

Figure 6. Aim29 senses the switch conformation of Zpr1•eEF1A•GTP. See also Figures S6 and S7.

(A) Ribbon diagram of ColabFold model showing eEF1A (colored by domain) bound to Aim29 (salmon) and the C-terminal half of Zpr1 (purple) with the N-terminal half of Zpr1 (residues 1-280) removed for clarity. The Switch I (SwI) of eEF1A and potential Aim29 interacting residues in stick representation are highlighted. The inset (rotated ~45° counterclockwise) shows the same Aim29 residues and neighboring eEF1A domain I residues within 5Å (blue). GTP (red) was modeled into the nucleotide pocket using AlphaFill. (B) Indicated strains carrying the Hsf1 reporter (4xHSE-YFP) were analyzed by

flow cytometry as described in Figure 1C. (C) FLAG IP analysis of cell lysates similar to Figure 3C but supplemented with GTP-γ-S as indicated and with a vector carrying the indicated 3xHA-Aim29 mutant. Dashes indicate cropping from the same immunoblot to remove irrelevant lanes. (D) FLAG IP of the indicated pure proteins and nucleotide similar to Figure 3D. Dashes indicate cropping from the same Coomassie-stained gel to remove irrelevant lanes. (E) Analysis of eEF1A trypsin resistance following *in vitro* translation for 15 minutes similar to Figure 2D. (F) Analysis of eEF1A release from Zpr1-3xFLAG beads similar to Figure 5A but with all samples incubated for 45 minutes. Dashes indicate cropping from the same immunoblot to remove irrelevant lanes.

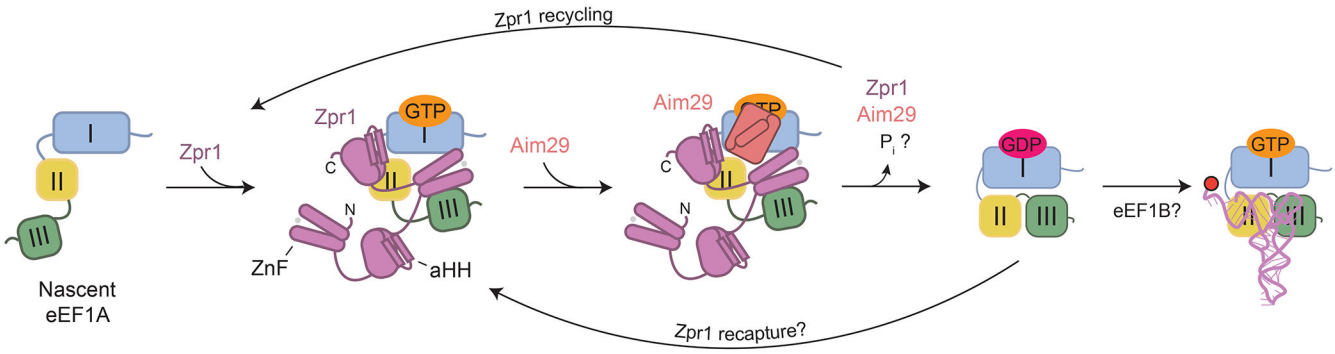

Figure 7. A mechanistic model for a GTPase folding cycle during eEF1A biogenesis.

Post-translational capture of an eEF1A folding intermediate by Zpr1 leads to GTPase activation. The GTP-bound conformational state of the Zpr1•eEF1A folding complex is sensed by Aim29. GTP hydrolysis in the presence of bound Aim29 destabilizes the folding complex, resulting in eEF1A release concomitant with Zpr1 recycling. eEF1A either matures into eEF1A(GTP)•aa-tRNA ternary complex or is recaptured by Zpr1 for another round of the GTPase folding cycle. Question marks indicate uncertainty about mechanistic contributions from phosphate release following hydrolysis and additional maturation factors. “ZnF” - zinc finger. “aHH” - alpha-helical hairpin. See Discussion for details.

KEY RESOURCES TABLE

REAGENT or RESOURCE	SOURCE	IDENTIFIER
Antibodies		
Goat-anti-rabbit IgG (H + L) HRP conjugate polyclonal	BioRad	Cat#1706515; RRID: AB_2617112
Goat-anti-mouse IgG (H + L) HRP conjugate polyclonal	BioRad	Cat#1706516; RRID: AB_2921252
Goat-anti-rabbit IgG IRDye 680LT polyclonal	LI-COR Biosciences	Cat#926-68021; RRID: AB_10706309
Donkey-anti-mouse IgG IRDye 680RD polyclonal	LI-COR Biosciences	Cat#926-68072; RRID: AB_10953628
Donkey-anti-mouse IgG IRDye 800CW polyclonal	LI-COR Biosciences	Cat#926-32212; RRID: AB_621847
Goat-anti-rabbit IgG IRDye 800CW polyclonal	LI-COR Biosciences	Cat#926-32211; RRID: AB_621843
Goat-anti-rat IgG IRDye 800CW polyclonal	LI-COR Biosciences	Cat#926-32219; RRID: AB_1850025
Rabbit-anti-hexokinase polyclonal	US Biological Life Sciences	Cat#H2035-03
Mouse-anti-PGK1 [22C5D8] monoclonal	ThermoFisher Scientific	Cat#459250; RRID: AB_2532235
Rabbit-anti-eEF1A polyclonal	Kerafast, Inc.	Cat#ED7001
Mouse-anti-FLAG M2 monoclonal	MilliporeSigma	Cat#F3165; RRID: AB_259529
Rabbit-anti-EIF2S1 phospho S51 [E90] recombinant (eIF2a phospho-Ser51)	Abcam	Cat#ab32157; RRID: AB_732117
Rat-anti-HA high affinity monoclonal (clone 3F10)	Roche	Cat#11867423001; RRID: AB_390918
Mouse-anti-ZPR1	ThermoFisher Scientific	Cat#MA1-13003; RRID: AB_10980362
Bacterial and Virus Strains		
Rosetta (DE3) *E. coli*	MilliPore Sigma (Novagen)	Cat#70954
Chemicals, Peptides, and Recombinant Proteins		
cOmplete™, Mini, EDTA-free Protease Inhibitor Cocktail tablets	Roche	Cat#04693159001
Pepstatin A	Roche	Cat#11359053001; CAS:26305-03-3
Phenylmethanesulfonyl fluoride (PMSF)	Sigma-Aldrich	Cat#78830; CAS:329-98-6
Dynabeads™ Protein G	Invitrogen	Cat#10004D
3xFLAG Peptide	Sigma-Aldrich	Cat#:F4799
GTP (sodium salt hydrate)	Roche	Cat#10106399001; CAS:36051-31-7
GDP (sodium salt)	Sigma-Aldrich	Cat#G7127; CAS:43139-22-6
GMP-PNP	VWR	Cat#76002-472; CAS:148892-91-5

REAGENT or RESOURCE	SOURCE	IDENTIFIER
GTP-γ-S	Abcam	Cat#:ab146662; CAS:94825-44-2
Micrococcal Nuclease	New England Biolabs	Cat#M0247S
RiboGuard™ RNase Inhibitor	Biosearch Technologies	Cat#RG90925
Turbo™ DNase	ThermoFisher Scientific	Cat#AM2238
Cycloheximide	MilliporeSigma	Cat#01810; CAS:66-81-9
Creatine Kinase	Roche	Cat#10127566001
Creatine Phosphate	Roche	Cat#10621714001; CAS: 71519-72-7
rATP, 100 mM	Promega	Cat#E6011
rGTP, 100 mM	Promega	Cat#E6031
Amino acid mixture, 1mM minus methionine	Promega	Cat#L9961
Sequencing Grade Modified Trypsin	Promega	Cat#V5113
Isopropyl-ß-D-thiogalactopyranoside (IPTG)- Dioxane free	US Biological Life Sciences	Cat#I8500; CAS: 367-93-1
Imidazole	Thermo Scientific Chemicals	Cat#A10221; CAS: 288-32-4
HisPur™ Ni-NTA Resin	ThermoFisher Scientific	Cat#88221
Benzonase Nuclease	MilliporeSigma	Cat#E1014
DEAE Cellulose resin	Biophoretics	Cat#B45059.02; CAS:9013-34-7
CM Sepharose Fast Flow	Cytiva	Cat#17071901
Tris(2-carboxyethyl)phosphine hydrochloride solution 0.5M pH 7.0 (TCEP)	MilliporeSigma	Cat#646547; CAS:51805-45-9
EGTA	Thermo Scientific Chemicals	Cat#J60767
Phosphatase Inhibitor Cocktail 3	Sigma-Aldrich	Cat#P0044
Stabilized EasyTag L-[35S]-Methionine	PerkinElmer	Cat#NEG709A
[14C(U)] Uridine diphosphate glucose	American Radiolabeled Chemicals, Inc.	ARC 0154
GTP, [α-^{32}P]- 3000Ci/mmol 10mCi/ml EasyTide	PerkinElmer	Cat#BLU506H250UC
TLC PEI Cellulose F	Millipore Sigma	Cat#105579
Critical Commercial Assays		
mMESSAGE mMACHINE™ T7 Transcription Kit	Invitrogen	Cat#AM1344
SuperSignal™ West Femto	Thermo Fisher Scientific	Cat#34095
GTPase Kinetic ELIPA Assay Kit	Cytoskeleton Inc.	Cat#BK052
Deposited Data		

REAGENT or RESOURCE	SOURCE	IDENTIFIER
Transcriptome profiling via RNA-seq of *AIM29* vs. *aim29*Δ vs. *aim29*Δ + *pmTDH3-ZPR1*	This study	GEO: GSE229425
Ribosome profiling of *aim29*Δ vs. *AIM29* cells	This study	GEO: GSE229777
Experimental Models: Organisms/Strains		
W303 MATa leu2-3,112 trp1-1 can1-100 ura3-1 ade2-1 his3-11,15	Solís et al., 2016	W303 (VDY465)
W303 MATa leu2-3,112::4xHSE-YFP::CgLEU2 trp1-1 can1-100 ura3-1 ade2-1 his3-11,15	Zheng et al., 2016	VDY3334
W303 MATa leu2-3,112::4xHSE-YFP::CgLEU2 trp1-1 can1-100 ura3-1 ade2-1 his3-11,15 aim29Δ::HIS3	This study	VDY5662
W303 MATa leu2-3,112 trp1-1 can1-100 ura3-1 ade2-1 his3-11,15 aim29Δ::HIS3	This study	VDY5670
W303 MATa leu2-3,112::4xHSE-YFP::CgLEU2 trp1-1 can1-100 ura3-1 ade2-1 his3-11,15 aim29Δ::HIS3 natMX::PrTDH3-ZPR1	This study	VDY5849
W303 MATa leu2-3,112::4xHSE-YFP::CgLEU2 trp1-1 can1-100 ura3-1 ade2-1 his3-11,15 natMX::PrTDH3-ZPR1	This study	VDY5850
W303 MATa leu2-3,112 trp1-1 can1-100 ura3-1 ade2-1 his3-11,15 aim29Δ::HIS3 natMX::PrTDH3-ZPR1	This study	VDY5851
W303 MATa leu2-3,112 trp1-1 can1-100 ura3-1 ade2-1 his3-11,15 ZPR1-3xFLAG::kanMX aim29Δ::HIS3	This study	VDY6197
W303 MATa leu2-3,112 trp1-1 can1-100 ura3-1 ade2-1 his3-11,15 TEF1-yeGFP::hphMX, HSP42-mCherry::HIS3	This study	VDY6230
W303 MATa leu2-3,112 trp1-1 can1-100 ura3-1 ade2-1 his3-11,15 TEF1-yeGFP::hphMX, HSP42-mCherry::HIS3 aim29Δ::URA3	This study	VDY6231
W303 MATα leu2-3,112::4xHSE-YFP::CgLEU2 trp1-1 can1-100 ura3-1 ade2-1 his3-11,15 aim29Δ::KlURA3 gcn2Δ::CgHIS	This study	VDY6293
W303 MATa leu2-3,112::4xHSE-YFP::CgLEU2 trp1-1 can1-100 ura3-1 ade2-1 his3-11,15 gcn2Δ::CgHIS	This study	VDY6295
W303 MATα leu2-3,112::4xHSE-YFP::CgLEU2 trp1-1 can1-100 ura3-1 ade2-1 his3-11,15 aim29Δ::KlURA3	This study	VDY6297
W303 MATα leu2-3,112 trp1-1 can1-100 ura3-1 ade2-1 his3-11,15 aim29Δ::CgHIS hsf1Δ::KAN pNH604-PrHSF1-HSF1(1-424)::TRP1	This study	VDY6300
W303 MATα leu2-3,112 trp1-1 can1-100 ura3-1 ade2-1 his3-11,15 hsf1Δ::KAN pNH604-PrHSF1-HSF1(1-424)::TRP1	This study	VDY6301
W303 MATa leu2-3,112 trp1-1 can1-100 ura3-1 ade2-1 his3-11,15 aim29Δ::CgHIS hsf1Δ::KAN pNH604-PrHSF1-HSF1::TRP1	This study	VDY6302
W303 MATa leu2-3,112 trp1-1 can1-100 ura3-1 ade2-1 his3-11,15 hsf1Δ::KAN pNH604-PrHSF1-HSF1::TRP1	This study	VDY6303
h^+ leu1-32 ade6-M216	Kind gift from Danesh Moazed	SPY76 (VDY5800)
h^- leu1-32 ade6-M216 ura4-D18 his3-Dr	Kind gift from Danesh Moazed	SPY79 (VDY5803)
h^+ leu1-32 ade6-M216 aim29Δ::kan^R zpr1-T353I	This study	VDY5819
h^+ leu1-32 ade6-M216 aim29Δ::kan^R pREP-ura4$^+$-ade6$^+$-P_{nmt1}-aim29-T_{nmt1}	This study	VDY5838
h^+ leu1-32 ade6-M216 aim29Δ::kan^R zpr1-T353I	This study	VDY5878
W303 MATa leu2-3,112::4xHSE-YFP::CgLEU2 trp1-1 his3-11,15 ura3Δ0 zpr1Δ::kanMX + pRS416 ZPR1	This study	VDY6319
W303 MATa leu2-3,112::4xHSE-YFP::CgLEU2 trp1-1 his3-11,15 ura3Δ0 zpr1Δ::kanMX aim29Δ::KlURA3 + pRS416 ZPR1	This study	VDY6320
W303 MATα leu2-3,112 trp1-1 can1-100 ura3-1 ade2-1 his3-11,15::pGAL-TEF1 tef2Δ::HIS3 ZPR1-3xFLAG::kanMX	This study	VDY6184
W303 MATa leu2-3,112::4xHSE-YFP::CgLEU2 trp1-1 can1-100 ura3-1 ade2-1 his3-11,15 aim29Δ::HIS3 tef1Δ::natMX	This study	VDY6269

REAGENT or RESOURCE	SOURCE	IDENTIFIER
W303 MATα leu2-3,112 trp1-1 can1-100 ura3-1 ade2-1 his3-11,15::pGAL-TEF1 tef2Δ::HIS3 ZPR1-3xFLAG::kanMX+ pRS416-*PrTEF2-TEF2-URA3*	This study	VDY6272
W303 MATα leu2-3,112 trp1-1 can1-100 ura3-1 ade2-1 his3-11,15::pGAL-TEF1 tef2Δ::HIS3 ZPR1-3xFLAG::kanMX+ pRS416-*PrTEF2-TEF2^{S53A}-URA3*	This study	VDY6273
W303 leu2-3,112 trp1-1 can1-100 ura3-1 ade2-1 his3-11,15 tef1Δ::natMX tef2Δ::HIS3 ZPR1-3xFLAG::kanMX+ pRS416-*PrTEF2-TEF2^{S53A}-URA3*	This study	VDY6279
W303 leu2-3,112 trp1-1 can1-100 ura3-1 ade2-1 his3-11,15 tef1Δ::natMX tef2Δ::HIS3 aim29Δ::HIS3 + pRS416-*PrTEF2-TEF2-URA3*	This study	VDY6281
W303 leu2-3,112 trp1-1 can1-100 ura3-1 ade2-1 his3-11,15 tef1Δ::natMX tef2Δ::HIS3 + pRS416-*PrTEF2-TEF2-URA3*	This study	VDY6282
Oligonucleotides		
GGGGGTAATACGACTCACTATAGGGAGAatttcatacacaatataaacgattgccaccATGGGTAAAGAGAAGTCTCAC	Sabbarini et al., 2023	oVD13102
TTTTTTTTTTTTTTTTTTTTTttacatctacactgttgttatcagtcgggcTCATTTCTTAGCAGCCTTTTGAGCAGCC	Sabbarini et al., 2023	oVD13103
TACCTCCCCCAAATTTTTTCTTGTTTGGTTGCATTATTTCcacaggaaacagctatgacc	This study	oVD11404
GCACTTACTTATTAATGAAGGCCATAAGCCAAACAACATCgttgtaaaacgacggccagt	This study	oVD11405
TTTTTAGAATATACGGTCAACGAACTATAATTAACTAAACCACAGGAAACAGCTATGACC	This study	oVD12116
GGTATATAAAAATATTATATGGAAGCAATAATTATTACTCGTTGTAAAACGACGGCCAGT	This study	oVD12117
CGCCGTACCACTTCAAAACACCC	This study	oVD13227
GAAAGCATAGCAATCTAATCTAAGTTTTAATTACAAAagatctGTTTAGCTTGCCTCGTC	This study	oVD13228
CGGGGACGAGGCAAGCTAAACagatctTTTGTAATTAAAACTTAGATTAGATTGCTATGC	This study	oVDD13229
GATCTGCCGGTCTCCCTATAGTGAGTCGTATTAGGAGATTGATAAGACTTTTCTAGTTGC	This study	oVD13230
AAAGATATGCAACTAGAAAAGTCTTATCAATCTCCTAATACGACTCACTATAGGGAGACC	This study	oVD13231
ACAAAATGCTTCACAACCCTGATG	This study	oVD13232
Recombinant DNA		
pRS414	Brachmann et al., 1998	pVD2766
pRS416	Brachmann et al., 1998	pVD2878
pRS424	Brachmann et al., 1998	pVD13
pRS414: *prTEF2-TEF2*	This study	pVD2858
pRS416: *prTEF2-TEF2*	This study	pVD2748
pRS416: *prTEF2-TEF2^{S53A}*	This study	pVD2749
pRS414: *prTEF2-TEF2^{D156N}*	This study	pVD2860
pRS414: *prTEF2-TEF2^{H95A}*	This study	pVD2904
pRS414: *prTEF2-TEF2^{H95N}*	This study	pVD2906
pRS414: *prAIM29-AIM29*	This study	pVD1898
pRS416: *prAIM29-AIM29*	This study	pVD1899
pRS414: *prTEF2-TEF2-EGFP*	This study	pVD2900
pRS414: *prTEF2-TEF2-EGFP^{D156N}*	This study	pVD2901

REAGENT or RESOURCE	SOURCE	IDENTIFIER
pmGCN4-EGFP	Kind gift from Onn Brandman	pVD2746
pRS416: *prTDH3-AIM29*	This study	pVD1967
pRS416: *prTDH3-ZPR1*	This study	pVD2891
pRS424: *pmZPR1-ZPR1*	This study	pVD2323
pRS416: *prAIM29-10xHis-3xFLAG-AIM29*	This study	pVD1895
pRS416: *prAIM29-10xHis-3xFLAG-AIM29^{K100A}*	This study	pVD2204
pRS416: *prAIM29-10xHis-3xFLAG-AIM29^{SwIMUT}(H53A, H97A, E133A, E135A)*	This study	pVD2822
pRS416: *prAIM29-3xHA-AIM29*	This study	pVD2871
pRS416: *prAIM29-3xHA-AIM29^{K100A}*	This study	pVD2872
pRS416: *prAIM29-3xHA-AIM29^{SwIMUT} (H53A, H97A, E133A, E135A)*	This study	pVD2873
pET28a: 6xHis-Lgt3	This study	pVD2736
pET16b: 10xHis-3C-ZPR1-3xFLAG	Sabbarini et al., 2023	pVD2627
pET16b: 10xHis-3C-ZPR1$^{ZnF\text{-}MUT}$-3xFLAG	Sabbarini et al., 2023	pVD2653
pET16b: 10xHis-2xHA-Aim29	This study	pVD2825
pET16b: 10xHis-2xHA-Aim29^{K100A}	This study	pVD2835
pET16b: 10xHis-2xHA-Aim29^{SwIMUT} (H53A, H97A, E133A, E135A)	This study	pVD2838
pET16b: 10xHis-2xHA-Aim29^{ZMUT} (K40A, S41A, Y44A, R45A, N46A, W155A)	This study	pVD2842
pREP *ura4^{+} ade6^{+} P$_{nmt1}$-aim29-T$_{nmt1}$*	This study	pVD2145
pRS414 *PrZPR1-ZPR1*	This study	pVD2592
pRS414 *PrZPR1-ZPR1^{T389I}*	This study	pVD2593
pRS424 *PrAIM29-C2ORF76*	This study	pVD1900
pREP *P$_{nmt1}$-3xFLAG-C2ORF76-T$_{nmt1}$* LEU2	This study	pVD2184
pREP *P$_{nmt1}$-ZPR1-T$_{nmt1}$* LEU2	This study	pVD2914
pREP *nmt1* LEU2	Kind gift from Danesh Moazed	pVD2042
pRS416: *prAIM29-10xHis-3xFLAG-AIM29^{S41A}*	This study	pVD2191
pRS416: *prAIM29-10xHis-3xFLAG-AIM29^{R45A}*	This study	pVD2193
pRS416: *prAIM29-10xHis-3xFLAG-AIM29^{N46A}*	This study	pVD2194
pRS416: *prAIM29-10xHis-3xFLAG-AIM29^{H97A}*	This study	pVD2203
pRS416: *prAIM29-10xHis-3xFLAG-AIM29^{E133A}*	This study	pVD2216
pRS416: *prAIM29-10xHis-3xFLAG-AIM29^{E135A}*	This study	pVD2218
pRS416: *prAIM29-10xHis-3xFLAG-AIM29^{W155A}*	This study	pVD2224
pRS416: *prAIM29-10xHis-3xFLAG-AIM29^{ZMUT}* (K40A, S41A, Y44A, R45A, N46A, W155A)	This study	pVD2834
pRS416: *prAIM29-3xHA-AIM29^{ZMUT}* (K40A, S41A, Y44A, R45A, N46A, W155A)	This study	pVD2874
pRS415:*prTEF2-TEF2-GFP*	This study	pVD2963
Software and Algorithms		

REAGENT or RESOURCE	SOURCE	IDENTIFIER
FastQC	https://github.com/s-andrews/FastQC	Version 0.11.5
STAR	Dobin et al., 2013	Version 2.7.0
DESeq2	Love et al., 2014	Version 1.34.0
Seqtk	https://github.com/lh3/seqtk	Version 1.3-r106
Cutadapt	https://github.com/marcelm/cutadapt	Version 2.0
deepTools	https://github.com/deeptools/deepTools	Version 3.3.0
DEGreport	https://github.com/lpantano/DEGreport	Version 1.30.0
BioConductor: flowCore	https://doi.org/10.18129/b9.bioc.flowcore	Bioconductor version: Release (3.15)
BioConductor: flowViz	https://doi.org/10.18129/b9.bioc.flowviz	Bioconductor version: Release (3.15)
Prism 9 for macOS	GraphPad	version 9.5.1
RiboToolKit	https://doi.org/10.1093/nar/gkaa395	
Other		
Whatman GD/X 25mm Syringe Filter, glass microfiber GF/D filtration medium	Cytiva	Cat#6888-2527
Whatman Type 1 filter paper	Cytiva	Cat#1001110